Semiconductor qubits in practice

Anasua Chatterjee[1], Paul Stevenson[2], Silvano De Franceschi[3], Andrea Morello[4], Nathalie P. de Leon[2] and Ferdinand Kuemmeth[1] ✉

Abstract | In the past decade, semiconducting qubits have made great strides in overcoming decoherence, improving the prospects for scalability and have become one of the leading contenders for the development of large-scale quantum circuits. In this Review, we describe the current state of the art in semiconductor charge and spin qubits based on gate-controlled semiconductor quantum dots, shallow dopants and colour centres in wide-bandgap materials. We frame the relative strengths of the different semiconductor qubit implementations in the context of applications such as quantum simulation, computing, sensing and networks. By highlighting the status and future perspectives of the basic types of semiconductor qubits, this Review aims to serve as a technical introduction for non-specialists and a forward-looking reference for scientists intending to work in this field.

The world of quantum devices has changed at a breakneck pace over the past two decades. In particular, the field has witnessed the development of a large variety of quantum bits or qubits, which are quantum, two-level systems whose state can be initialized, coherently controlled and measured with high fidelity. Increasing research efforts are focusing on physical implementations and materials offering the best prospects for large-scale integration. Correspondingly, scaling and engineering efforts are increasingly moving from academic research labs to industrial-scale development centres. Semiconductor materials have been at the forefront of these developments, along with other quantum technologies based on trapped ions and superconducting circuits.

Quantum applications will be far-reaching and will depend strongly on the specific properties of the underlying quantum hardware. Therefore, the focus of this Review goes beyond quantifying the merits of different semiconductor qubits as per their potential role in universal quantum computers. We also explore their relevance for different applications that make use of their quantum character, including sensing, simulation, computation and communication.

The field of semiconductor qubits itself spans a variety of systems, material implementations and techniques. The semiconductor qubits demonstrated so far differ from each other in various ways; they vary from systems that operate at millikelvin temperatures, achievable only inside dilution refrigerators, to systems that are suitable for room-temperature operation. They can be artificially engineered potential wells confining quantized electronic states or single-atom impurities in a lattice, exploiting either nuclear or electronic degrees of freedom. Despite these differences, however, they share certain properties, such as their potential for high-density integration on a large scale, which originates from the well-established nanofabrication technology of the semiconductor industry. Some semiconductor qubits also boast some of the longest coherence times ever reported. Following material and technology developments in the past few years, silicon spin qubits were able to meet all of the DiVincenzo criteria[1], and paradigmatic, two-qubit quantum algorithms have been demonstrated. Colour centres have demonstrated long-range entanglement generation capabilities[2] and have shown themselves to be sensitive probes for nanoscale magnetometry at room temperature[3,4], with particular relevance for biological and medical applications.

This Review reflects the wide variety of platforms offered by different semiconductor qubit systems. Because of the extremely rapid growth of this area in the past few years, here, we summarize the state of the art of the field, rather than its historic development, with emphasis on relating different categories of semiconducting qubit implementations to their respective strengths and prospects for practical applications. Specifically, we will describe semiconductor qubits based on charge and spin degrees of freedom. Among spin-based qubits, we shall devote the most attention to gate-controlled quantum dots (QDs), dopants and colour centres, with the qubit encoded in an individual electronic or nuclear spin. We briefly touch upon other qubit realizations where quantum information is encoded in a multielectron state, such as the singlet-triplet qubit, the hybrid spin-charge qubit or the flip-flop spin qubit. We shall not discuss the case of semiconductor self-assembled QDs, on which extensive literature can be found

[1] Center for Quantum Devices, Niels Bohr Institute, University of Copenhagen, Copenhagen, Denmark.

[2] Department of Electrical Engineering, Princeton University, Princeton, NJ, USA.

[3] Univ. Grenoble Alpes and CEA, IRIG/PHELIQS, Grenoble, France.

[4] Centre for Quantum Computation & Communication Technology, School of Electrical Engineering & Telecommunications, University of New South Wales (UNSW), Sydney, NSW, Australia.

✉ e-mail: kuemmeth@nbi.dk

https://doi.org/10.1038/s42254-021-00283-9

Key points

- Semiconductor qubits span an entire ecosystem and are extremely versatile in terms of quantum applications, particularly viewed through the lenses of quantum simulation, sensing, computation and communication.
- Controlling the charge degree of freedom in gated quantum dots is important for sensing of quantum objects, readout and light–matter coupling.
- Gate-controlled spin qubits have demonstrated long coherence times, fast two-qubit gates and fault-tolerant operation, with promising prospects for quantum computation.
- Shallow dopants have shown some of the longest coherence times in the solid state and high sensitivity to magnetic fields, relevant for quantum memories and sensing.
- Optically active defects have shown great promise as in situ sensors, and their natural ability to serve as spin–photon interfaces makes them suitable for long-distance quantum communication.
- Looking beyond a fault-tolerant quantum computer, semiconductor qubits will find diverse applications such as light–matter networks, scanning sensors, quantum memories, global cryptographic networks and small-scale designer simulation arrays.

(these systems are particularly relevant for the realization of single-photon sources[5]). In the interest of concision, we also exclude from this Review gatemon qubits and topological qubits, even though semiconductors are at the heart of their operating principles. We refer to recent reviews for superconducting qubits[6] and Majorana zero modes[7], respectively.

Each qubit category is benchmarked against four quantum technology applications (see FIG. 1). In quantum sensing applications, some observable of the qubits is sensitive to the desired environmental variable, without perturbing it in a manner that cannot be corrected for. In quantum simulations, the Hamiltonian of a physical system of interest is mapped onto the Hamiltonian of an appropriately controlled qubit circuit. For quantum computing applications, we assess the fidelity, prospects for two-qubit control and coherence time of the qubit. For quantum communication, semiconductor qubits can serve as nodes in quantum networks, enabling non-classical communication between distant sites. Examples of the materials systems, readout and manipulation methods for the semiconducting qubits discussed in this Review are illustrated in FIGS 2,3,4, respectively and some quantities of interest are summarized in TABLE 1. A future outlook for semiconductor qubits is provided in FIG. 5.

Gate-defined quantum dots

In a semiconductor structure, the location and motion of an individual electronic charge can be controlled and measured with relative ease, and it can also be used to encode a qubit. In this section, we discuss a family of semiconductor-based QDs where the confinement of electrons (or holes) is obtained through electrostatic gating in combination with physical or band-structure confinement, and where qubit states can be encoded in the charge or spin degrees of freedom, or combinations thereof.

The first QD devices of this family were made from arsenic-based III–V heterostructures (III = Ga, In, Al and V = As) typically grown by molecular-beam epitaxy[8]. A particularly successful approach relied on the use of modulation-doped GaAs/AlGaAs heterostructures hosting a high-mobility two-dimensional electron gas (2DEG). In this case, vertical confinement (along the growth direction) occurs at the GaAs/AlGaAs heterojunction, due to a conduction-band step of a few hundred meV. Lateral confinement is obtained by means of metallic gate electrodes fabricated on the semiconductor surface, which deplete the 2DEG to form a small isolated puddle of electrons.

Because of its versatility, this approach is widely used to reliably realize tunable single QDs or small tunable arrays of tunnel-coupled dots. The key to this success lies in the low defect density of the epitaxially grown heterostructures and in the relatively low effective mass of electrons in GaAs, which favours quantum confinement. Moreover, because the 2DEG lies typically 50–100 nm below the surface, the QD confinement potential is relatively insensitive to surface charges. The occupation of gated QDs can be tuned down to the few-electron regime. The exact electron number can be measured by means of a nearby charge sensing device, that is, another QD or a quantum point contact[9]. Increasing the complexity of the gate layout allows going from one single QD to two or more QDs tunnel-coupled by gate-tunable interdot barriers (see example in FIG. 1).

GaAs-based heterostructures have played a pivotal role in the development of QD devices, but much of the research focus is now shifting towards silicon-based nanostructures, owing to their potential for spin-based quantum computing. Isotopically purified silicon, enriched in nuclear-spin-free ^{28}Si, has been shown to provide long spin lifetimes, as discussed in the next section. In addition, silicon is an attractive material for large-scale integration using industrial production processes. Due to the larger effective masses in silicon, however, the characteristic size of the QDs needs to be smaller than in GaAs, that is, less than ~20 nm, which poses nanolithographic challenges. Currently, foundry-fabricated silicon-on-insulator transistor technology (incorporating gates over a silicon nanowire, see FIG. 2a) and devices fabricated from high-mobility Si/SiGe strained heterostructure (see FIG. 2b) show promise for industrial mass production, at least on the single-qubit and two-qubit levels.

Charge control and coherence

A single electron trapped in a pair of adjacent QDs can encode a charge-based qubit. The two basis states correspond to the electron being localized either on the left or on the right QD (labelled $|L\rangle$ or $|R\rangle$, respectively), from which bonding and antibonding combinations are formed in the presence of interdot tunnelling. We label them as $|0\rangle$ and $|1\rangle$, respectively. FIGURE 4a shows the energy-level structure of the double QD as a function of the detuning parameter, ε, defined as the energy difference between states $|L\rangle$ and $|R\rangle$ in the limit of vanishing coupling. Due to interdot tunnelling, the two states hybridize, forming bonding and antibonding combinations with minimal energy splitting, $2t$, where t is the tunnelling amplitude. After initializing the qubit in the $|R\rangle$ state, coherent charge oscillations can be induced by a non-adiabatic gate voltage pulse (shown in red in FIG. 4a) towards $\varepsilon \approx 0$ for a controlled amount of time.

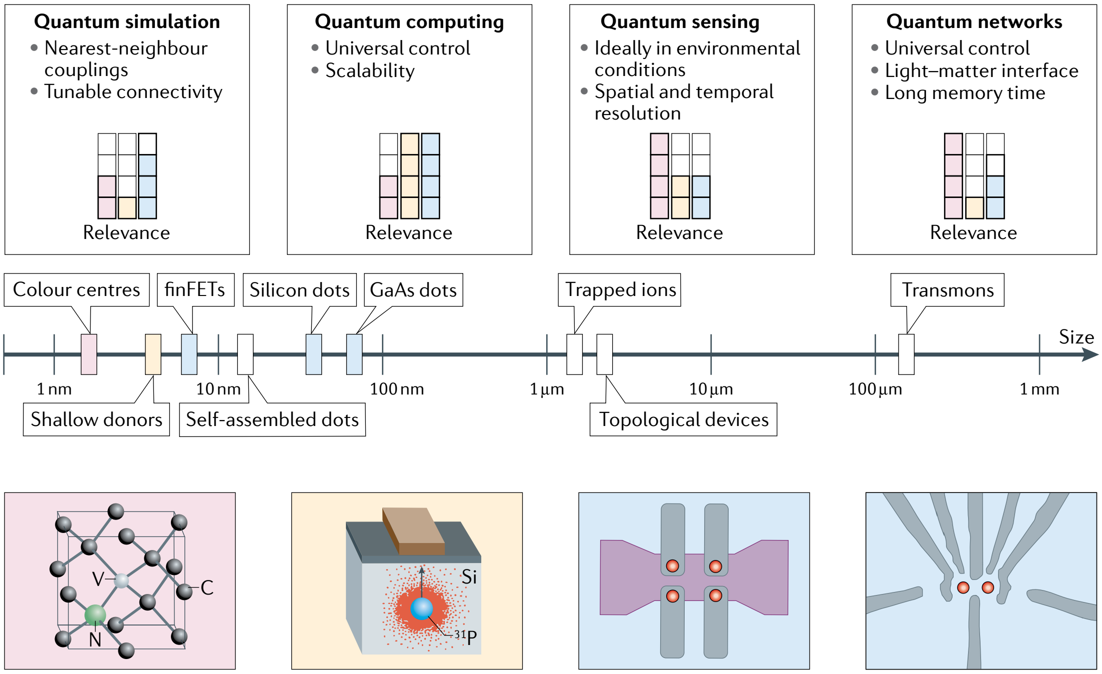

Fig. 1 | **Semiconductor qubits and their potential applications.** Top: four areas of quantum applications, with different desired features and their suitability to a particular physical implementation (denoted by the colour of the boxes in the bottom graphic). For the purposes of quantifying a system for quantum simulation (as opposed to potential for fault-tolerant quantum computation), we have considered the ability to deterministically place and control the interactions of a set of quantum objects (spin, charge and so on) to simulate specific physical models, ideally with a simpler architecture and lower effort than that required for a universal quantum computer. Centre: various solid-state qubit implementations arranged by the approximate size of the qubits' active parts, not including readout ancilla and sensing devices. Bottom: representative illustrations of the four major qubit categories covered. From left to right, in order of the qubit size: colour centres (pink box), shallow dopants (yellow box) and gate-patterned quantum dots (silicon-on-insulator accumulation-mode and GaAs depletion-mode devices; blue boxes). finFET, fin field-effect transistor.

Initially, these oscillations were measured in electron transport, manifesting as periodic modulations of the current through the double QD as a function of the pulse duration, t_p (REF.[10]). Successively, they were detected by measuring the charge occupation of the double QD via a nearby charge-sensitive device, such as a quantum point contact or another QD[11], see FIG. 3a. The latter approaches eventually enabled a demonstration of full charge qubit functionality with two-axis control[12]. Another type of charge-based qubit was experimentally demonstrated in a silicon double QD confining electrons. Such an alternative qubit exploits the multi-valley nature of the silicon conduction band. In a silicon QD, spatial confinement results in a partial lifting of the sixfold valley degeneracy, leaving two lowest energy valleys separated by an energy gap, the so-called valley splitting, that can vary between a few and hundreds of µeV. In the case of a relatively small valley splitting, the QD state can be brought into a superposition of the two valley components. Coherent valley-state oscillations[13] and, eventually, a valley qubit with two-axis control[14] were demonstrated in a silicon double QD. Qubit readout was realized by projecting the valley states onto different charge configurations of the double QD, which were measured with a nearby charge sensor. Although the charge qubits discussed above allow for extremely fast quantum operation, they are generally sensitive to charge noise, which makes their coherence time rather short and limits the number of consecutive coherent rotations that can be realized. The detrimental effect of charge noise can be partly mitigated by operating the qubit in a regime where the energy difference between bonding and antibonding states is first-order insensitive to electric field fluctuations. In the case of the valley qubit, this occurs at large detuning, where the coherence time can reach several nanoseconds[14]. In the case of conventional charge qubits, which rely on a single excess charge shared between two adjacent QDs, the sweet spot is at $\varepsilon \approx 0$, where the energy difference between the bonding and antibonding states is first-order insensitive to charge noise (that is, to fluctuations in ε). Reference[11] reported a maximum coherence time of about 7 ns at $\varepsilon = 0$, comparable to that of valley qubits.

Further improvements in the sweet-spot coherence time can be achieved through material optimization and device engineering. Reference[15] reported a coherence time of 0.4 µs in a silicon-based double QD fabricated from a strained Si/SiGe heterostructure similar to the one shown in FIG. 2a. A similarly long coherence time was obtained[16] using a double QD defined in a GaAs/AlGaAs heterostructure.

Although charge makes it difficult to engineer long-coherence qubits for quantum applications, it provides an easily accessible tool for the readout of other qubit encodings using spin-to-charge conversions

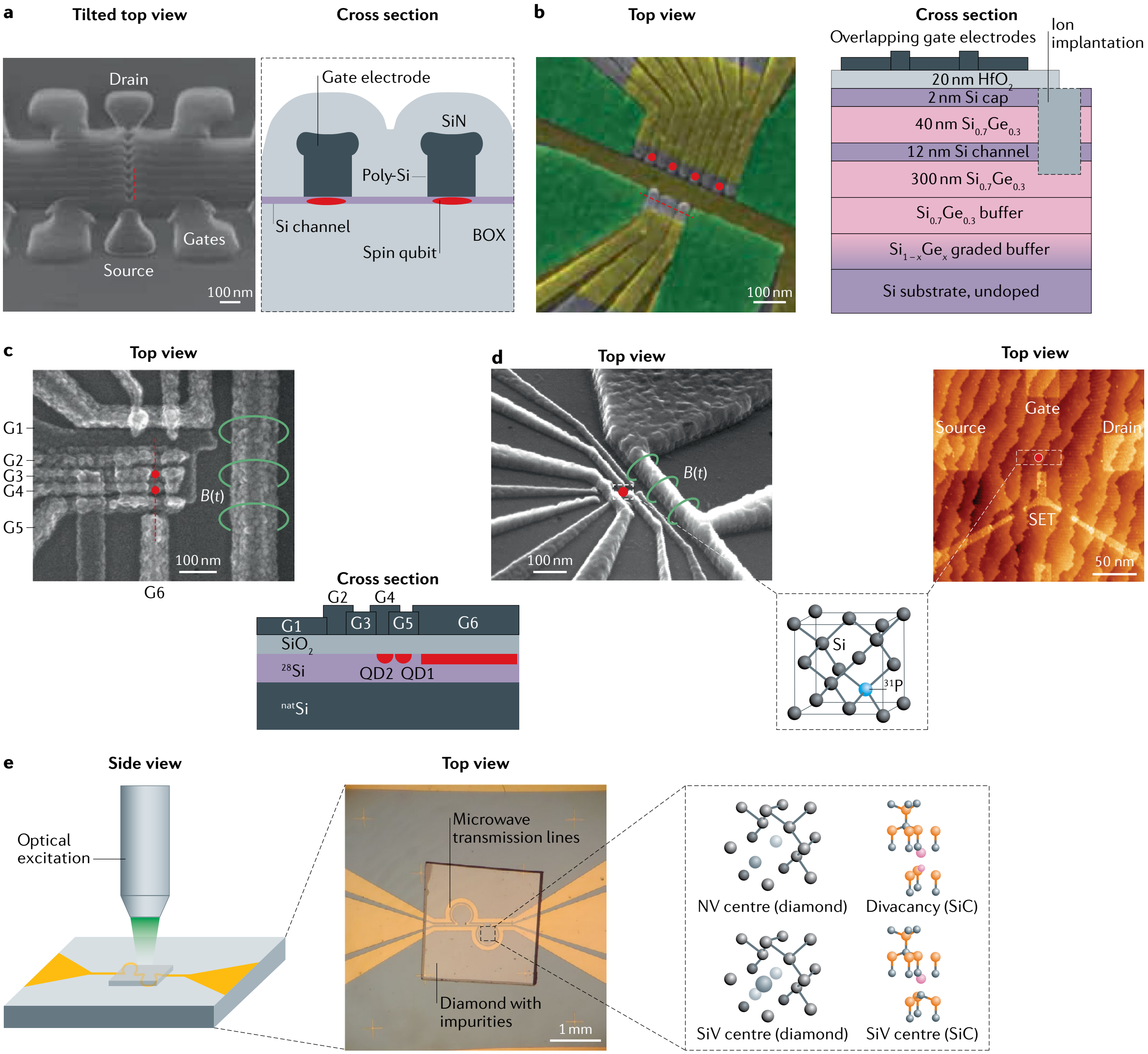

Fig. 2 | **Material systems hosting semiconductor qubits. a** | Quantum dots in nanowires. The confinement is provided in 2D by the structure of the nanowire itself (materials may be germanium, InAs, silicon and so on), whereas gate electrodes below or above the nanowire create a confining potential along the nanowire. Shown here are fin field-effect transistor-like gates overlapping a silicon nanowire in a silicon-on-insulator device[63], in top view and cross section (partial, of section indicated by the red line in the top view). The buried silicon oxide insulator layer is labelled BOX. **b** | Heterostructured materials, typically grown by molecular beam epitaxy or chemical vapour deposition. Here, a silicon–germanium heterostructure is shown in cross section, with a graded buffer for relieving strain and using band structure engineering to create quantum wells[279]. Another well-known example is GaAs. Gates are patterned on top (shown in top view) to confine carriers within the plane of the quantum well; two or three layers of overlapping gates (adjacent gates false-coloured in yellow are patterned on different layers, in addition to the green screening layer) can greatly enhance confinement and control[85]. **c** | A planar silicon structure can also be used, with overlapping aluminium gates confining carriers to form qubit dots or single-electron transistors (SETs)[28], as shown in top view and cross section. $B(t)$ is the magnetic field (marked by green field lines) and G1...G6 denote the gates; QD1 and QD2 denote the two quantum dots. **d** | Shallow dopants can be implanted into a suitable crystal (here, phosphorus, a dopant with an extra electron, into silicon, as shown in the inset) with a gate above the implantation location for tuning of the dopant's chemical potential. Gates (here, for an SET charge sensor) can be patterned on top of the crystal as for gate-patterned quantum dots, to read out the dopant charge or spin state[82], or couple it with a quantum dot. Another approach (right panel) involves engineering the silicon surface atom-by-atom, placing dopant atoms for qubits (with source and drain reservoirs, as well as a gate for local control), SET and gates[121], as shown in the top-view scanning tunnelling microscope image of the silicon surface. **e** | Optically active point defects can be addressed by a combination of confocal microscopy and microwave manipulation (left). Substitutional defects and vacancies are common motifs in these defects, such as the nitrogen-vacancy[164] and silicon-vacancy centres[213] in diamond and the divacancy[220] and silicon-vacancy[174] complexes in silicon carbide (right). Panel **a** image courtesy of Louis Hutin (CEA-Leti). Panel **b** left side is adapted with permission from REF.[279] and the right side image is courtesy of Fabio Ansaloni, Niels Bohr Institute. Panel **c** image courtesy of Andrew Dzurak. Panel **d** is adapted with permission from REFS[82,121].

(see below). These remarkable advances in single-carrier control have been instrumental in establishing a strong quantum-mechanical coupling between a semiconductor charge qubit and the photon field of a superconducting microwave resonator, opening the door to circuit quantum electrodynamics with semiconductor–superconductor systems[17–20].

Spin-based qubits

Localized spins in semiconductors provide natural implementations of two-level systems for qubits[21]. Although the individual electronic (or nuclear) spins of dopants embedded in semiconductors can serve as ultra-coherent quantum bits (see the next section), in this section, we focus on gate-controlled QDs, where

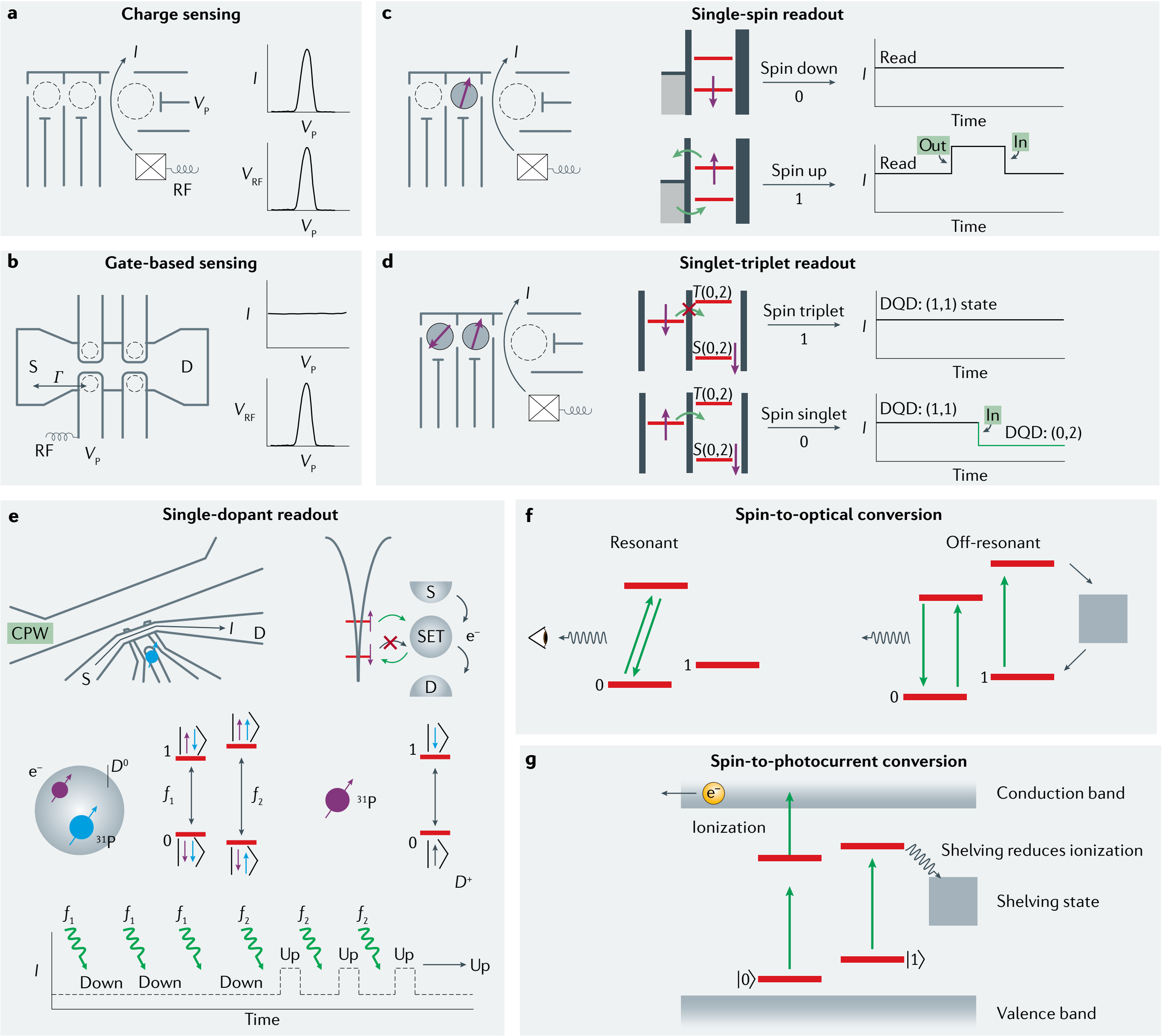

Fig. 3 | **Readout techniques for semiconductor qubits.** BOX 1 includes further details about each readout method. Proximal (panel **a**) and gate-integrated (panel **b**) charge sensors for readout of charge and spin qubits in gate-controlled semiconductor quantum dots. Γ indicates the tunnel rate between the quantum dot and the reservoir. I stands for a DC current flowing through the sensor, which is sensitive to charge rearrangements in its environment as a plunger gate is varied (V_P). Alternatively, V_{RF} stands for the reflectometry signal (typically derived from a carrier in the radio-frequency (RF) range) that is used to read out the sensor with high bandwidth (about 10 MHz). The signal is usually dependent on the tunnel rate (Γ) to the source (S) or drain (D). Readout mechanisms for two common qubit encodings, the single-spin qubit (panel **c**, 'Elzerman readout') and the singlet-triplet (S–T) spin qubit (panel **d**, Pauli spin blockade). DQD refers to double quantum dot. **e** | Readout of shallow dopants using the DC current I running through a single-electron transistor (SET) charge sensor. Dopant energy levels (D^+) and (D^0) form the two-level system for the ionized nuclear spin and the electron spin qubit, respectively. Transitions are addressable using distinct frequencies (f_1 and f_2) delivered via a coplanar waveguide (CPW). **f** | Spin-to-optical readout for colour centres. The qubit states 0 and 1 can be distinguished by detecting the presence or absence of fluorescence, using either resonant or non-resonant optical excitation. **g** | Spin-to-photocurrent readout for colour centres. In the presence of optical drive fields (green arrows), qubit states 0 and 1 lead to drastically different electrical current that can be detected in the conduction band, due to the presence of shelving states that suppress ionization for the 1 state.

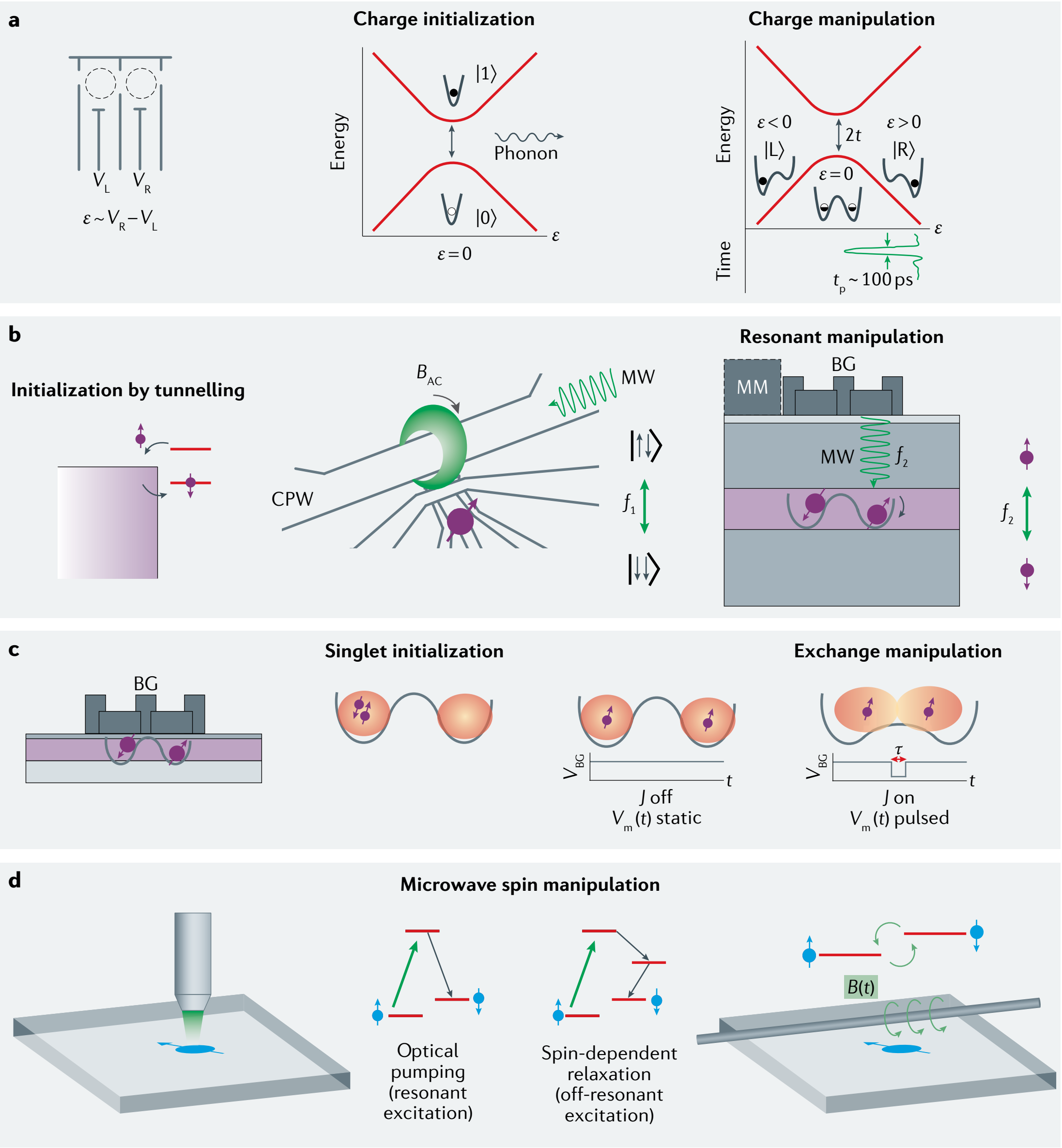

Fig. 4 | **Manipulation methods for semiconducting qubits.** Depending on the materials system and qubit encoding, a host of initialization and manipulation methods is available. **a** | For charge, voltage pulses applied to gate electrodes can reconfigure potentials in short timescales. Voltages (V_L and V_R, where subscripts L and R stand for left and right, respectively) applied to the gate electrodes can move an electron to the left or to the right, or delocalize it over the two quantum dots, creating bonding and antibonding orbitals (separated in energy by the tunnel coupling, *t*), by tilting the potential over picosecond timescales ((t_p), right panel). Relaxation via phonon emission can be employed to initialize the qubit. **b** | For a single spin, initialization can be performed by aligning the two Zeeman-split levels with a reservoir such that (as shown here) only the down spin can tunnel onto the quantum dot or dopant. Resonant manipulation can be performed via precisely timed AC fields, which can be magnetic (B_{AC}), directly driving the spin via a microwave (MW at frequency f_1) stripline (coplanar waveguide, CPW, left panel), or electric, shaking the position of the spin in natural[69] or synthetic[25] (micromagnet-generated, see square labelled MM, right panel) spin–orbit fields (at frequency f_2). **c** | The Heisenberg exchange interaction can be used to rotate spins by a specified amount, by finely tuning the degree of wavefunction overlap[34]. This can be done on fast timescales (~ps to ns), using gate voltage pulses; for example, by lowering the barrier gate (BG, left panel) in the case of symmetric operation[45], the exchange interaction (*J*) can be turned on for a time τ. For three spins instead of two, exchange-based gates can provide for universal one-qubit and two-qubit operations[42,44]. Initialization can be performed by loading the two spins into a single dot and waiting for relaxation into the singlet ground state. **d** | Optical pumping provides a convenient route to initializing optically active defects in a specific state, while resonant microwave fields allow for coherently controlling different spin projections (green arrows, right panel).

slow and fast gate voltages are used to confine and manipulate either electron or hole spins. As for the case of charge-based qubits, the need to overcome the thermal energy and suppress phonon-assisted excitations limits qubit operation to very low temperatures. Even though most of the experiments so far were performed below 100 mK (hence, requiring dilution refrigerators), qubit functionality above 1 K has been recently

Decoherence-free subspace
A subspace of the qubit's Hilbert space where it is decoupled from specific environmental noise, leading to an evolution that is close to completely unitary; characterized as passive error correction.

demonstrated[22,23]. In few-electron QDs, the electron spin has shown long coherence times[24]; in materials with a low natural density of spinful nuclei, such as silicon, isotopic purification has enabled researchers to achieve dephasing times, T_2^*, routinely exceeding tens of microseconds (and, occasionally, even up to 120 μs (REF.[24]), which is much longer than manipulation times[25].

Various spin-based qubit encodings exist, and, in the last decade, spin qubits involving more than a single electron have been shown to offer advantages such as electrical control and decoherence-free subspaces. However, trade-offs in terms of increased operational complexity and fabrication overhead can be involved. Here, we describe a few qubit encodings of particular interest.

- The single-spin (Loss–DiVincenzo) qubit[21]: in the presence of a static magnetic field, the Zeeman-split $|\uparrow\rangle, |\downarrow\rangle$ spin states of an unpaired electron confined in a QD form a paradigmatic qubit encoding. A time-dependent modulation of a magnetic field perpendicular to the one that creates the static energy splitting provides a means to execute coherent single-qubit operations[24,26]. Exchange-based two-qubit gates can be executed by controlling the wavefunction overlap associated with two spins[27,28]. In addition to singly occupied QDs, larger (odd) occupation numbers have also been explored[29–31], and may offer advantages in terms of electrical screening[32] or as intermediate-range couplers[33].
- The singlet-triplet qubit: the qubit is encoded in the singlet ($|S\rangle = (|\uparrow\downarrow\rangle - |\downarrow\uparrow\rangle)/\sqrt{2}$) and unpolarized triplet ($|T_0\rangle = (|\uparrow\downarrow\rangle + |\downarrow\uparrow\rangle)/\sqrt{2}$) states of two electrons in a double QD. Here, the qubit splitting can be set and controlled by the gate voltages[34–36]. Coherent rotations can be achieved via a magnetic field gradient between the dots, while an orthogonal rotation axis about the Bloch sphere is provided by the finite exchange energy[37]. The qubit can be operated in the symmetric regime, for example, by applying control voltage pulses to the interdot potential instead of the detuning to reduce noise[38–41]. With a magnetic quantum number $m_s = 0$ for both qubit states, the qubit is also robust against global magnetic field fluctuations.
- The exchange-only qubit: using three electrons in a triple QD[42–44], this qubit provides two axes of rotation via the gate-voltage-controlled exchange interaction, mitigating the need for a magnetic field gradient, at the cost of more complex operation and a heightened sensitivity to charge noise. For sufficiently large interdot tunnelling, these devices can be operated in a rotating frame as resonantly driven exchange (RX) qubits[19,42,45]. Three-electron spin qubits have been reviewed in detail in REF.[46].
- The charge-spin hybrid qubit[47]: demonstrated as an all-electrical, double-dot, three-electron qubit with fast rotations (π-rotations within 100 ps), the hybrid qubit combines advantages from its charge-like (speed) and spin-like (increased coherence) nature.
- Multi-dot spin qubits: generalizing the singlet-triplet and exchange-only qubits to collective spin states of multi-dot systems, the quadrupolar exchange-only[48] qubit and the exchange-only singlet-only[49] qubit were recently proposed. Both of them exploit a decoherence-free subspace at an extended charge sweet spot and can potentially be operated fast, either resonantly or via electrical voltages.

Table 1 | **Current state of the art for semiconductor qubits**

Qubit type	Characteristic timescales (s)		Quantum computation		Quantum sensing	
	T_1	T_{2DD}	Single-qubit gate time	Single-qubit fidelity	Quantity	Sensitivity
Gated charge	30 ns (REF.[273])	7 ns (REF.[11])	~0.1 ns (REF.[12])	86%[273]	Charge	~10^{-4} e/$\sqrt{(\text{Hz})}$ at 1 Hz (REF.[11])
Gated spin	57 s (REF.[54])	28 ms (REF.[24])	25 ns (REF.[25])	99.96%*[274]	Magnetic field gradients	50 pT/$\sqrt{\text{Hz}}$ (REFS[24,167])
Shallow dopants (electron)	>1 h (REF.[101]) (ens), 10 s (REF.[120])	10 s (REF.[104]) (ens), 0.56 s (REF.[124])	~100 ns (REF.[82])	99.94%*[127]	Magnetic field (AC)	18 pT/$\sqrt{\text{Hz}}$ (REF.[124])
Shallow dopants (nucleus)	>days[66]	3 h (REF.[111]) (ens), 35.6 s[124]	~20 μs (REF.[66])	99.98%*[126]	Magnetic field (AC)	2 nT/$\sqrt{\text{Hz}}$ (REF.[131])
Colour centres	>1 h (NV⁻ diamond)[175]	1 s (NV⁻ diamond)[175]	<20 ns (REF.[173])	99.995%* (NV⁻ diamond)[275]	Magnetic field (DC)	50 pT/$\sqrt{\text{Hz}}$ (REF.[244]) (ens), 500 nT/$\sqrt{\text{Hz}}$ (REF.[243])
					Magnetic field (AC)	32 pT/$\sqrt{\text{Hz}}$ (REF.[276]) (ens), 4.3 nT/$\sqrt{\text{Hz}}$ (REF.[245])
	10 s (SiV SiC)[277]	>20 ms (SiV SiC)[277]		99.984%* (divacancy SiC)[221]	Temperature	100 mK/$\sqrt{\text{Hz}}$ (REFS[250,251]) (SiV in diamond, SiC)
					Electric field	10^{-5} V · μm^{-1} / $\sqrt{(\text{Hz})}$ (REF.[278])

We provide the best known values (at the time of writing) for key single-qubit timescales: the relaxation time, T_1, and the maximum coherence time, T_{2DD}, using dynamical decoupling. For quantum computation, we quote the typical single-qubit gate time and the highest single-qubit gate fidelity; an asterisk denotes gate fidelities assessed using randomized benchmarking and (ens) indicates values obtained in bulk spin ensembles. State-of-the-art experiments for quantum sensing are also highlighted, in terms of the quantity sensed and the sensitivity achieved. For gated charge, the reported timescales refer to experiments on semiconductor double quantum dots operated as charge qubits. Yet, much longer sweet-spot coherence times (around 0.4 μs) were found in double quantum dots coupled to a superconducting resonator[15,16]. We also note that charge sensitivity is frequency dependent due to the $1/f^{\gamma}$ character of electrical noise ($0.7 \lesssim \gamma \lesssim 1.4$ (REFS[270–272])), and it can be measured in different device set-ups. For example, measurements on singlet-triplet qubits yielded a spectral density of 2×10^{-8}e/$\sqrt{\text{Hz}}$ at 1 MHz (REF.[272]). When scaled down to 1 Hz, this value is consistent with the one given in the table. Unless otherwise noted, quantum sensing metrics for colour centres refer to the negatively charged nitrogen vacancy centres (NV⁻) in diamond. SiV and SiC stand for silicon vacancy and silicon carbide, respectively.

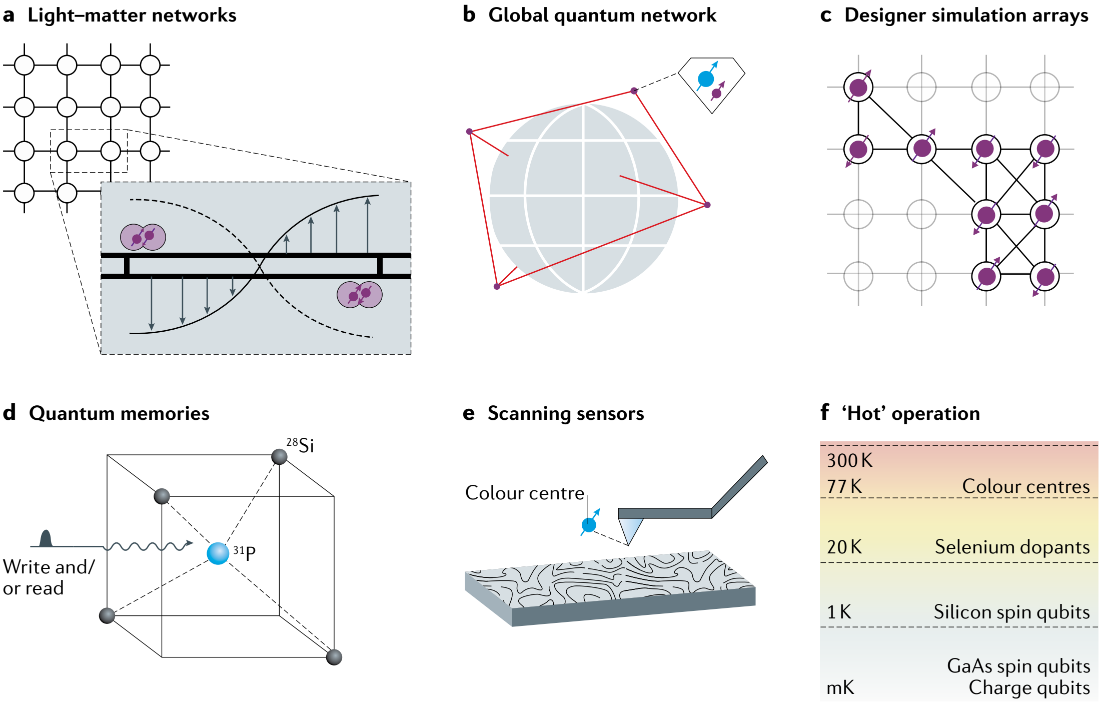

Fig. 5 | **Future outlook for semiconductor qubits.** The applications for semiconductor qubits are diverse, and we illustrate only a few here. **a** | The demonstration of strong coupling between microwave photons and charge or spin qubits in gate-controlled systems underpins the field of hybrid systems that blend light and matter, or superconductor–semiconductor networks. The inset shows a network with local nodes consisting of quantum-dot-based spin qubits coupled via a superconducting resonator. **b** | Colour centres have made headway towards quantum networks, with the ability to entangle distant qubits across hundreds of kilometres. Other uses include entanglement beacons for cryptography and secure global communications. **c** | Quantum-dot-based arrays of spin qubits have been used for proof-of-principle simulations of condensed-matter systems such as the Hubbard model and Nagaoka ferromagnetism. 2D arrays and arbitrary connections could enable versatile, reconfigurable simulations. **d** | Dopants in silicon have shown extraordinary coherence times and are among one of the best candidates for addressable quantum memories and dense qubit arrays. **e** | Colour centres fabricated on the tip of a scanning probe can be used for extremely sensitive magnetometry across surfaces. **f** | An attractive proposal is the operation of qubits at temperatures reachable without dilution refrigerators or even at room temperature. Although most gate-controlled spin and charge qubits require millikelvin temperatures, spins in silicon have been operated as qubits above 1 K, whereas selenium dopants in silicon are predicted to be operable above 77 K. Colour centres can be operated at room temperature.

Apart from the electron spin, confined holes[50–52], that is, missing valence band electrons, provide for the realization of another kind of spin qubit, one where the contact hyperfine interaction is suppressed owing to the p-wave symmetry of valence band states (reviewed recently[53] in the context of the material system germanium). Here, intrinsic spin–orbit interaction is sufficiently strong to enable hole spin rotations driven by purely electrical means.

Initialization, readout and manipulation

Usually, qubit initialization is not performed by thermalization to the spin ground state, since spin relaxation times can be in the range of seconds or even up to a minute[54]. Therefore, faster methods are used, such as hotspot thermalization[22] or initialization by aligning a particular level of the two-level system to a reservoir (spin-selective tunnelling)[28]. For the singlet-triplet qubit, the singlet state is most easily initialized in the (2,0) charge state, whereas adiabatic separation into the (1,1) state would initialize the ground state in the nuclear basis ($|\uparrow\downarrow\rangle$ or $|\downarrow\uparrow\rangle$)[34]. (In this notation, numbers indicate the occupation of the left and right wells of a double QD.) Currently, gate-controlled spin qubits[55] can be initialized with fidelities above 99%.

Despite the multiple ways of encoding the spin qubits described above, the primary readout method is based on spin-to-charge conversion[56]. Whereas the magnetic moment of a single spin is exceedingly small (on the order of the Bohr magneton, ~57.8 μeV T^{-1}) and its direct detection is correspondingly difficult, the detection of small displacements of charge has been perfected over the years. Techniques based on a local charge detector[34], radio-frequency reflectometry[57,58] or dispersive readout via a resonator[59,60] have been developed (see FIG. 3a,b). To implement spin-to-charge conversion, a charge displacement between dots, or between a QD and a reservoir, is engineered to be dependent on the spin-qubit state (see BOX 1). For spin qubits in particular, the Pauli spin blockade[61], where the Pauli exclusion principle ensures that charge tunnelling is blocked or allowed based on the spin state of the qubit, has been widely utilized across material systems. A separate charge detector can be used for this measurement; this can be a constriction

Set of universal quantum gates
A set of quantum gates to which all other quantum operations can be reduced.

Qubit Larmor frequency
Frequency of the spin qubit, rotating via Larmor precession along a static magnetic field in the laboratory frame.

Dynamical decoupling
Applying periodic sequences of short qubit control pulses, with an intended effect of approximately averaging out the unwanted system–environment coupling. Common sequences are the Hahn echo, CPMG and XYXY.

in a nearby 2DEG, called a quantum point contact[62], a QD[45], a single-electron transistor (SET)[24] or a direct measurement of charge hybridization by detecting the associated changes in gate capacitances[29,57,60,63,64]. Charge detectors in conjunction with spin-to-charge conversion and radio-frequency reflectometry have yielded single-shot spin-state measurements in microseconds[59], whereas high readout fidelities have been reported both for dot-based (99.86%)[65] and for dopant-based nuclear (99.8%)[66] and electron spins (99.8%)[67].

In order to form a set of universal quantum gates, for each encoded qubit, methods are required for individual rotations about two axes of the Bloch sphere and for creating entanglement between two neighbouring qubits. Typically, for gate-controlled spin qubits, these logic gates are achieved by two methods.

Directly engineered magnetic fields, turned on and off for short timescales using a coplanar stripline fabricated adjacent to the spin qubit, can be used to perform single-spin rotations via electron spin resonance[24,26]. This method involves using resonant microwave pulses that match the qubit Larmor frequency, thereby, driving rotations between the energy levels.

Fast gate-voltage pulses can be used to move the electron or hole wavefunction or to electrostatically change their effective charging energies. Such baseband pulses are, therefore, useful to switch on and off the Heisenberg exchange interaction (FIG. 4c), allowing to coherently control singlet-triplet and exchange-only qubits. Microwave-modulated pulses are used to spatially oscillate the electron wavefunction, thereby, generating effective time-varying magnetic fields via natural[68–72] or synthetic[73–75] spin–orbit fields (FIG. 4b, right). The result is a form of spin resonance that involves an electric dipole transition, thus, called electric dipole spin resonance.

Box 1 | Spin-to-charge conversion

For spin qubits in semiconductors, measurements of the spin state are typically made through projection onto another degree of freedom such as charge, which is more easily accessible by transport and charge-sensing measurements. Spin-to-charge conversion has become the dominant way to read out QD spin states. Here, we illustrate this principle for a few different qubit implementations.

- FIGURE 3c shows a sketch of spin-to-charge conversion based on energy selection. A single spin in a QD is capacitively coupled to a sensor and tunnel-coupled to a reservoir. After spin manipulation, the dot energy level is tuned such that the Fermi reservoir lies between the two Zeeman-split spin states (↑ and ↓). If the dot is in state ↓, the Coulomb blockade prevents the electron from entering the reservoir, whose energy levels are completely filled at that energy, and there is, therefore, no charge rearrangement and no change in the sensor signal. For a state ↑, the electron can tunnel out of the QD and into empty states of the reservoir located above the Fermi energy, leading to a measurable charge change until a new electron tunnelling in reinitializes the qubit to its ground state.
- For a double-dot singlet-triplet qubit, capacitively coupled to a sensor, the conversion process makes use of spin-to-charge conversion (FIG. 3d). Here, the two levels are the singlet ($|S\rangle$, typically in the (0,2) charge state) and the (1,1) triplet state ($|T_0\rangle$). After spin manipulation in the (1,1) charge state (that is, with one electron in each QD), gate voltages are adjusted to favour the (0,2) charge state. If the two spins are singlet-correlated (antisymmetric spin states), the left electron can tunnel to the same orbital occupied by the right electron, giving rise to a charge change detected by the sensor. If the two spins are parallel (symmetric spin states), the Pauli exclusion prevents such a tunnelling, unless higher-lying orbitals in the right dot can be accessed. This conditional tunnelling process arising from spin blockade is known as spin-to-charge conversion.
- Shallow dopants also use the process outlined for single-spin state conversion to charge. However, in all qubit demonstrations to date, a single-electron transistor acts both as the charge sensor and as the charge reservoir for spin-to-charge conversion. The dopant energy levels that form the two-level system for the ionized nuclear spin and the electron spin qubit are shown in FIG. 3e, and transitions are addressable using distinct frequencies (f_1 and f_2 in the figure). After manipulation, as described for the first case, the dopant energy levels are aligned with the single-electron transistor, and conditional tunnelling is used to both measure and reinitialize the qubit.
- In colour centres, spin-to-charge conversion can be used either as a direct readout scheme (via photocurrent) or as a contrast mechanism. Both schemes rely on state-dependent photoionization; in the case of the negatively charged nitrogen-vacancy (NV^-) centre in diamond, shelving into a metastable singlet state protects the $m_s = \pm 1$ states from ionization. The resulting photocurrent can be measured directly with local electrodes, or the ionization into the spectrally distinct NV^0 charge state may be used to increase contrast in traditional photoluminescence-based readout schemes.

Material systems

There are several material systems suitable for gate-controlled spin qubits, with specific advantages and disadvantages for particular applications. These include engineered heterostructures (where charge carriers are strongly confined along the growth directions), nanowires (which naturally provide confinement in two directions) and planar semiconductor platforms (see FIG. 2).

Starting in 2005, the first experiments demonstrating spin qubits were reported in GaAs/AlGaAs heterostructures[34], where the 2DEG formed in the GaAs layer was depleted by negative gate electrodes to trap individual electrons for qubit operations. The GaAs platform benefits from a relative simplicity of fabrication and some favourable electronic properties, such as a single conduction band valley and a small effective mass leading to less stringent lithographic constraints. That said, the totality of the atoms in the lattice carry a non-zero nuclear spin, making hyperfine interaction a significant source of decoherence and leading to intrinsic inhomogeneous dephasing times of $T_2^* \approx 10\,\text{ns}$. However, more than a decade of technological improvements in GaAs, namely, the development of nuclear field distribution narrowing by dynamic nuclear polarization[37] and dynamical decoupling sequences[76], have enabled millisecond-long coherence times[76] and single-qubit control with a fidelity of 99.5% (REF.[77]). Additionally, piezoelectricity and spin–orbit coupling are other concerns in this material system, while the direct bandgap could potentially be useful for spin–photon conversion for readout or other applications based on optical access. Currently, research continues on GaAs heterostructure-based devices for proof-of-concept multi-spin quantum devices[33,78,79], spin transfer demonstrations[80] and quantum simulators[81].

Since the demonstration of the first[82,83] silicon spin qubits in 2012, the research focus has moved to this low-nuclear-spin material system. Here, electrons (or holes) are confined in the silicon in metal–oxide–semiconductor (MOS) devices with either planar[24] or nanowire[51,84] structures, or in devices based on silicon–germanium (Si/SiGe) heterostructures[47,74,75,85]. Dopant atoms in the silicon host can also be used as qubits[66,82], as discussed in the next section.

Natural silicon contains only 4.7% of ^{29}Si, the only stable isotope bearing nuclear spin; this can be reduced to ppm concentrations by isotopic purification[86]. Silicon also has a weaker spin–orbit interaction than GaAs, InAs and InSb, and is a material compatible with powerful foundry fabrication in the microelectronics industry.

Currently, silicon spin qubits have some of the longest coherence times among spin qubits, with gate-controlled implementations showing a (dynamically decoupled) coherence time up to 28 ms (REF.[24]). However, some challenges remain[87]: in silicon, devices need to be smaller compared with GaAs devices, due to the larger effective mass of electrons, and fabrication results are not yet as reproducible as in GaAs. As a result of valley degeneracy, low-lying leakage states can exist and they may be thermally populated even at low temperature[87]. In the future, research on silicon qubits must focus on the scalability considerations due to the fact that valley splitting is affected by unavoidable fabrication-related defects, inhomogeneities and step edges in the nanowire, interface or heterostructure. Encoding spin qubits in hole-based QDs is a possible approach to overcome such issues, since the topmost valence band comprises only one valley.

Germanium, another group IV semiconductor and the material of the first transistor, has been used to make SiGe/Ge/SiGe quantum-well heterostructures confining high-mobility hole gases and QDs that can be used to encode spin qubits[50,52,53,88]. Due to the inherent presence of a sizeable spin–orbit coupling in the valence band, hole qubits can be manipulated by means of electric dipole spin resonance without the need for local micromagnets. The characteristic manipulation times demonstrated so far (~10 ns) are shorter than those typically achieved for electrons, which partly compensates for the shorter hole coherence times.

Applications

Quantum sensing. Spin qubits are well suited for quantum sensing since they are sensitive magnetometers and excellent detectors for charge noise if operated appropriately. For example, gate-tuned exchange interactions can be finely dependent on electrical fields and are, thereby, useful to detect both low-frequency and high-frequency electrical signals. In the magnetic domain, the nuclear spin bath and its diffusion constant has been measured using the dephasing of a spin qubit in GaAs (REF.[89]). However, impurity atoms such as shallow donors or negatively charged nitrogen-vacancy (NV^-) centres are currently more suited to technologies such as scanning-probe magnetometers. In the future, flip-chip technology[90], already available for gate-controlled superconducting qubits, could open up applications where a gate-controlled charge or spin qubit, operated as a sensor, could be scanned over another material surface. In addition, through fast spin-to-charge conversion techniques, spin qubits can be local probes for other physical systems that can also be implemented in semiconductors, such as nanowires and high-mobility 2DEGs. When these systems interact in specific ways with spin, they can be probed in a range of bandwidths; examples include the Kondo state, quantum Hall edge states and topological entities such as Majorana fermions[91]. However, the requirement for millikelvin temperatures and wiring requirements, combined with the lack of optical addressability, make it difficult for these spin systems to be useful for biological or environmental sensing.

Quantum simulation. A primary characteristic of gate-controlled QDs is their versatility and ability to realize 2D arrays[78] to engineer and simulate specific Hamiltonians. Owing to their superior coherence, spin-based encodings offer a better prospect as opposed to their charge counterparts. The gate-controlled exchange interaction for spin can be used to form as-desired nearest-neighbour connections in a spin qubit array, which can be controlled on nanosecond timescales (see FIG. 5c). Arrays of spin qubits have lent themselves to simulation experiments, such as that of a Mott insulator based on the Hubbard model[92] and for probing itinerant magnetism in the Nagaoka regime[81].

Quantum computation. Along with superconducting qubits and trapped ions, gate-controlled spin qubits are one of the technologies that present an advanced level of development with regards to coherence, scalability and the ability to make small-scale quantum processors, making quantum computation one of the primary long-term applications of these systems[93,94]. With a greater research focus on the silicon material system, especially with semiconductor companies and research foundries entering the fray, foundry-fabricated silicon qubits are becoming a reality and demonstrating the scalability of the gate-controlled approach. At the same time, SiGe and planar silicon devices have shown long coherence times, especially impressive when compared with short gating times, yielding gate fidelities above some error correction thresholds. Finally, with the demonstration of reliable two-qubit gates[28,52,75,95], all of the DiVincenzo criteria[1] have been satisfied and simple proof-of-principle quantum algorithms[95] have been implemented.

Quantum networks. Quantum communication involves non-classical communication based on entanglement shared over large distances, whether directly or through an intermediary classical or quantum system. For spin qubits, direct entanglement is a difficult goal to achieve, since the long coherence times of spins are due to their isolation from the environment, and spin–spin interactions are intrinsically short-ranged. However, intermediary systems have been used to extend the range of this interaction over longer distances. One way is to use an exchange coupling mediated via a large multielectron dot[33]. Another way is to physically shuttle electrons[96] using a surface acoustic wave or finely tuned and timed voltage pulses[97]. An opportunity for long-distance coupling is coming from circuit quantum electrodynamics using superconducting resonators. Originally developed for charge qubits, this approach could be extended to spin qubits by means of spin-charge hybridization[17–19,98,99]. This is currently a very active field of research[20]. Finally, the direct gap in GaAs and other materials could be useful for a direct exciton-to-optical-photon coupling.

Summary

By leveraging the electronic spin degrees of freedom and properly engineered spin-charge hybridization schemes, gate-defined QDs are capable of long coherence times, along with fast, gate-controlled manipulation and readout techniques, with prospects for a scalable, all-in-one platform with low overhead per qubit. This is further enhanced by advances in silicon qubit technology, achieving compatibility with industrial semiconductor fabrication. The versatility of qubits and qubit arrays formed by a wide range of gate geometries, when combined with a library of different qubit encodings, also makes them useful to study small-scale simulations and condensed matter systems.

Dopants in silicon

Shallow group V donors in group IV materials constitute a solid-state analogue of the hydrogen atom. For example, phosphorus in silicon (Si:P) possesses a weakly bound electron in a 1s-like orbital wavefunction and a spin-1/2 nucleus coupled to the electron via Fermi contact hyperfine interaction. The 1s orbital envelope wavefunction has a Bohr radius of about 2 nm: an estimate for this value could be obtained from the hydrogen Bohr radius formula $a_0 = 4\pi\varepsilon_0\hbar^2/m_e e^2$, replacing the permittivity of vacuum ε_0 with the dielectric constant of silicon and the electron mass m_e with the effective mass m^* of an electron near the bottom of the silicon conduction band.

Looking beyond the hydrogen atom approximation, the physics of spin and orbital states of shallow donors reveals important details on band structure properties, such as valley degeneracy of the conduction band minima, spin–orbit coupling or valley–orbit coupling. Therefore, at the dawn of modern semiconductor electronics, detailed studies of the quantum properties of dopant atoms in silicon[100] constituted an important benchmark for band structure theories, which were being developed in the 1950s. It was well known, even back then, that the spins of electrons bound to dopants in silicon possess long-lived quantum states[101].

Once quantum computing became a topic of active research, it was, therefore, natural to consider donor spins for quantum information processing. In a similar spirit as the earlier Loss–DiVincenzo proposal for quantum computing with spins in QDs[21], Bruce Kane presented a proposal to encode quantum information in the nuclear spin of individual ^{31}P donor atoms in silicon[102]. Kane warned about the extreme technological challenge in fabricating devices at the single-atom level, but argued that the progress in miniaturization imposed on the semiconductor industry by the pursuit of Moore's law would eventually lead to the capacity to fabricate silicon devices at the scale necessary for quantum computing. Twenty years later, this vision has indeed materialized.

Spin coherence in donor ensembles

The renewed interest in the spin coherence of donors in silicon motivated a series of electron spin resonance studies on bulk spin ensembles, particularly as a function of isotopic enrichment of ^{28}Si. Samples with residual ^{29}Si (with nuclear spin $I = 1/2$) concentration of 800 ppm showed electron coherence times $T_{2e} \approx 60$ ms (REF. [103]), extensible to 10 s by suppressing dipole–dipole interactions[104–106] and further reducing the ^{29}Si concentration to 50 ppm. The accuracy of these experiments made them an ideal test bed for advanced theoretical methods to describe spin dephasing caused by a fluctuating nuclear spin bath[107]. Such highly coherent spins systems enabled the demonstration of a nuclear quantum memory protocol, where the electron spin state is stored in the ^{31}P nucleus and later retrieved[108]. Operating at high magnetic field (3.4 T) and low temperature (2.9 K) allowed for the establishment of genuine quantum entanglement between the electron and the nuclear spin of the P donors[109]. Using the spin-dependent photoionization of the donors to detect the nuclear spin polarization, donor ensembles in highly enriched ^{28}Si exhibited extraordinary nuclear coherence times, $T_{2n}^{0} = 3$ min in the neutral charge state[110] and $T_{2n}^{+} = 3$ h in the ionized state[111], all obtained using XYXY dynamical decoupling.

The integration of donor ensembles with superconducting resonators allowed the observation of the Purcell effect, that is, cavity-enhanced relaxation, in the electron spins of ^{209}Bi donors[112].

Initialization, readout and manipulation

A scalable quantum processor requires individually addressable and measurable donors. The fabrication of single-donor devices can take two alternative pathways: one based on hydrogen lithography with scanning tunnelling microscopy (STM)[113] and the other following the industry-standard ion implantation method[114]. The first experimental breakthrough in this field was achieved by combining MOS QDs[115] with ion-implanted donors in a tightly integrated structure, in which a large QD acts as a tunnel-coupled charge sensor for the donor-bound electron. Using the energy-dependent tunnelling method developed earlier in GaAs QDs[56] unlocked the capability to read out the spin state of a single electron spin on an implanted P atom in single shot[116]. The same method was later applied to STM-fabricated donor clusters[117], and extended to fast spin detection with a radio-frequency SET[118]. Donor-based QDs (each containing approximately 3–4 STM-placed P donors) were used to demonstrate single-gate dispersive readout of singlet-triplet spin states[119].

The spin-lattice relaxation time T_1 of donor-bound electrons is strongly dependent on magnetic fields, with $T_1^{-1} \propto B^5$ (REF. [116]), and also influenced by confinement and proximity of metallic gates[120]. The longest observed single-donor T_1 is 9.8 s at $B = 1$ T. For a single electron bound to a 3P donor cluster, the deeper confining potential allowed T_1 to extend to 30 s (REF. [121]) at $B = 1.5$ T. A value of $T_1 \approx 5{,}000$ s was observed at $B = 0.32$ T in donor ensembles[101].

The coherent control of single-atom electron[82] and nuclear[66] spin qubits in silicon was achieved by integrating an implanted ^{31}P atom with the readout circuitry and a broadband, on-chip microwave antenna. The first experiments, conducted using a natural Si substrate, yielded spin coherence times in line with the expectations from ensemble experiments, with electron dephasing time $T_{2e}^{*} = 55$ ns and Hahn echo time $T_{2e}^{\mathrm{H}} = 200$ µs (REF. [82]).

Hahn echo time
Decoherence time obtained via a Hahn echo sequence, a form of dynamical decoupling of the qubit from its environment.

Clifford gate
The Clifford gates are quantum gates from the Clifford group affecting permutations of Pauli operators; examples are the Hadamard gate, the CNOT gate and the X, Y, Z gates.

Spin-squeezed states
Special kinds of entangled states that allow us to go beyond the classical projection noise limit due to the independent nature of single spins; useful for quantum sensing using interferometry.

Kicked-top model
A well-studied model of single-body quantum chaos, the dynamics of the kicked top is described by a time-dependent Hamiltonian combining the top's spin precession with nonlinear periodic 'kicks'.

Trotter steps
In digital quantum simulation, the time evolution of a simulation (*t*) is often decomposed into *n* Trotter steps of duration *t*/*n*, called the 'kicking period' for the kicked-top model.

The Hahn echo times for a single ^{31}P nuclear spin in natural silicon are $T_{2n0}^{\mathrm{H}} = 3.5$ ms and $T_{2n+}^{\mathrm{H}} = 60$ ms in the neutral (D^0) and ionized (D^+) states, respectively[66]. Measuring nuclear coherence times in diluted donor ensembles is extremely challenging, but a value of $T_{2n0}^{\mathrm{H}} = 16.7$ ms was obtained using hyperpolarized neutral donors[122] and a value of $T_{2n+}^{\mathrm{H}} = 18$ ms was obtained in ionized donors using electrically detected magnetic resonance[123].

With the introduction of isotopically enriched ^{28}Si substrates, the performance of single-donor qubits improved dramatically, with coherence times reaching $T_{2e} = 0.56$ s and $T_{2n}^{+} = 35.6$ s using dynamical decoupling[124]. These record coherence times translate to one-qubit Clifford gate fidelities, measured by randomized benchmarking of 99.94% for the electron[125] and 99.98% for the nucleus[126]. Electron-nuclear entanglement, mediated by the hyperfine interaction, was demonstrated by violating Bell's inequality with a record Bell signal $S = 2.70$ (REF. [127]).

Alternative dopant atoms

Although the majority of research on shallow donors has focused on ^{31}P in silicon, alternative dopants offer interesting properties. ^{209}Bi possesses a large nuclear spin $I = 9/2$ and a very strong hyperfine interaction $A = 1.4$ GHz, which result in an energy-level diagram that comprises 'clock transitions', that is, pairs of states whose energy splitting is first-order insensitive to magnetic field noise[128]. Ensembles of ^{209}Bi atoms have been integrated with superconducting resonators to obtain the first demonstration of the Purcell effect for spins in the solid state[112]. Integrating a single ^{123}Sb donor (nuclear spin $I = 7/2$) in a nanoscale device has led to the discovery of nuclear electric resonance, whereby coherent nuclear spin transitions are induced by the electrical modulation of the nuclear quadrupole coupling[129]. Acceptor atoms such as boron have been recently studied in ensemble experiments using planar microwave cavities and have shown remarkably long spin coherence times ($T_2^{\mathrm{CPMG}} \approx 10$ ms) in strained samples of enriched ^{28}Si (REF. [130]).

Applications

Quantum sensing. The high spin coherence of donors in enriched ^{28}Si translates into a high sensitivity to minuscule magnetic field perturbations[131]. Noise spectroscopy on a single ^{31}P atom revealed a noise floor equivalent to $18\,\mathrm{pT}/\sqrt{\mathrm{Hz}}$ (REF. [124]). However, the need for low-temperature operation and integration with charge readout devices suggests that the magnetic sensing applications of donors are likely to be limited to the detection of materials and structures fabricated directly on top of the chip.

Recently, the idea of sensing strain at the atomic scale has been suggested[131]. Strain is universally adopted in modern ultra-scaled silicon transistors to maximize their electrical performance. Lattice strain could be detected either through its influence on the quadrupolar splitting of heavy group V donors such as ^{75}As (REF. [132]) and ^{123}Sb (REF. [129]) or through the shift of the optical transition frequency of the erbium atoms[133].

The recent demonstration of full quantum control of a high-spin ^{123}Sb nucleus[129] opens exciting perspectives for exploring highly non-classical spin states for quantum sensing. Enhanced quantum sensing methods pioneered in the cold atoms community[134] include the use of Schrödinger cat states or spin-squeezed states. Their metrological usefulness is a topic of active research, as it depends crucially on the nature of the noise that perturbs the system. It is predicted that the key to achieving a metrological advantage from non-classical spin states is the presence of non-Markovian noise[135], which is precisely the kind naturally occurring in solid-state spins immersed in a nuclear spin bath[136–138].

Quantum simulation. The atomic size and amenability to atomically precise placement makes dopants in silicon an appealing platform to embody solid-state quantum simulations of the Hubbard model, where single-site measurement could be obtained by STM[139]. In the context of digital quantum simulations, efficient methods for discretizing quantum dynamics is an active research topic. For example, quantum simulations of the kicked-top model may provide precious insights into the proliferation of errors due to discrete Trotter steps[140]. A proposal suggests that a chaotic top can be experimentally implemented in the high-spin nucleus of a ^{123}Sb donor[141].

Quantum computation. Dopant spins in silicon are among the most coherent quantum systems in the solid state, but building a scalable quantum processor requires moving beyond single-spin coherence and one-qubit gate fidelities, introducing a coupling between the electrons. The natural coupling mechanism is the exchange interaction[21,102], arising from overlap of the donor electron wavefunctions. Strong exchange has been observed in several two-donor devices[142,143], and fast time-resolved exchange oscillations have been achieved using donor-defined QDs, with $t_{\sqrt{S}} = 0.8$ ns for a $\sqrt{\mathrm{SWAP}}$ operation[144]. In the regime where the exchange is weaker than the electron-nuclear hyperfine coupling[145], a native controlled-rotation gate can be implemented using fixed exchange coupling and state-conditional microwave pulses[146]. The very short range and oscillatory behaviour[147] of this interaction, however, poses significant challenges to the layout of a large-scale processor. Therefore, there have been suggestions for spacing out the donors using large interposer QDs[148], dopant spin chains[149] or ferromagnetic couplers[150].

Alternatively, scaling up donor-based quantum computers might be achieved by adopting different qubit encodings that possess an electric dipole and use electric dipole–dipole interaction, or coupling the dipole to a microwave resonator to achieve long-distance coupling. A natural system in which an electric dipole can be dynamically induced is the boron acceptor. Placing B in strained Si creates a noise-resilient system[130], where theory predicts that dipole–dipole coupling can mediate a two-qubit gate (the $\sqrt{\mathrm{SWAP}}$ gate) between acceptor spins in 4 ns at 20-nm distance[151].

A large artificial electric dipole can be induced on a ^{31}P donor by placing it at a vertical distance ≈15 nm from a Si/SiO$_2$ interface and applying a vertical electric field to displace the donor-bound electron towards the interface[152]. This introduces a strong electrical modulation of the electron-nuclear hyperfine coupling, which can be used to electrically drive coherent transitions between the $|\Uparrow\downarrow\rangle \leftrightarrow |\Downarrow\uparrow\rangle$ 'flip-flop' states. Theoretical models predict that a pair of flip-flop qubits could perform $\sqrt{\mathrm{SWAP}}$ operations in 40 ns at a distance of 200 nm (REF.[153]).

A hybrid donor-dot system can also be used in a two-electron configuration to form a singlet-triplet qubit. The magnetic field gradient ΔB_z is set to a fixed and large value by the presence of the hyperfine coupling in the donor-bound electron. Fast exchange oscillations, with $t_{\sqrt{S}} = 4$ ns, were observed experimentally in a hybrid device comprising a MOS QD and an implanted donor[154].

In addition to the coupling methods discussed above, some proposals provide detailed prescriptions for the layout and operation of large-scale, donor-based quantum computers, where multi-qubit gates are mediated by magnetic dipole coupling[155], by a moving probe[156] or by shuttling electrons across QDs coupled to sub-surface donors[157]. For donor encodings that possess an electric dipole, there is also the theoretical option of achieving long-distance coupling mediated by microwave photons in superconducting resonators[151,153].

The atomic, identical nature of the dopant atoms is ideal to explore quantum computing schemes involving spin ensembles[131]. For example, donor ensembles could be used as a spin-wave memory element in a quantum Turing machine[158].

Quantum networks. The indirect bandgap of silicon is normally an obstacle for the establishment of optical interconnects between shallow donors, since the decay of an optical excitation typically results in an Auger process, where the energy of the absorbed photon is imparted to the donor-bound electron, instead of being re-emitted. More promising systems for the spin-optical interface are group VI donors such as ^{77}Se, which have much deeper binding potentials than shallow group V atoms, and possess optical resonances in the mid-infrared, associated with long-lived spin states and magnetic clock transitions[159]. Such optically addressable donors have been theoretically considered in the context of 3D cluster-state quantum computing, with qubits coupled via integrated photonics[160].

Alternatively, rare-earth atoms such as erbium exhibit spin-dependent optical transitions at telecommunication wavelength and have been integrated with nanoscale transistors for electrical readout of the optical excitation[161].

Summary

Dopants in silicon provide an eclectic platform for quantum technology applications[131]. They offer outstanding spin coherence times and the choice of compatibility with standard silicon MOS fabrication pathways or near-atomic placement precision using STM lithography. Their atomic nature enables a broad range of experiments both at the single-atom level and in large ensembles.

Optically addressable quantum defects

Optically addressable quantum defects are point defects in a lattice where a spin degree of freedom is coupled to one or more optical transitions. This spin–photon interface allows for the combination of two powerful toolkits: spin resonance techniques for manipulating the spin and its interactions with its environment, and single-molecule microscopy techniques for addressing individual quantum defects. The electronic spin sublevels of an atom-like qubit serve as the qubit states, similar to dopants in silicon. The optical manifold serves a dual role as both a control and a readout mechanism. There has been intense interest over the past two decades in developing quantum defects for a variety of technologies, with notable success in colour centres in diamond and silicon carbide (SiC), and rare-earth ions (REIs) in various crystal hosts. Such defects have been deployed in a number of quantum applications, including spin–spin entanglement[162–165], nanoscale and quantum sensing[3,4,166–169], and remote entanglement and quantum teleportation[2,170]. These atomic-scale defects share many of the advantages and applications explored in strain QDs[171], with the advantage of the long spin coherence times achievable in nuclear-spin-free host materials.

Initialization, manipulation and readout

A combination of optical and microwave manipulation of quantum defects allows for full control of the spin. Quantum defects can be initialized into a well-defined ground state by various optical pumping schemes. For room-temperature operation, off-resonant excitation and spin-projection-dependent inter-system crossings can be used to initialize the system[172]. This approach presents a simple route to initialization outside the low-temperature regime, but the fidelity is limited by the inter-system crossings rate contrast. At low temperatures, excitation of non-cycling fine-structure transitions may be used for high-fidelity (>99.7%) initialization[173]. In the case of defects with non-integer spins $S > 1/2$, it may be necessary to simultaneously drive spin transitions in order to create a well-defined initial state[174]. Coherent control of the spin qubit is commonly achieved using microwave pulses (drawing on similar pulsed techniques used in essentially all solid-state qubit platforms), delivered by a wire loop antenna or stripline resonator, to directly drive transitions between spin states. The wide availability of ultra-stable commercial microwave sources enables the use of long dynamical decoupling sequences to extend coherence times[175].

Optical readout is one of the key advantages of optically addressable quantum defects, enabling the qubit to function as a spin–photon interface. Long-distance quantum communication requires flying qubits, and contact-free readout is highly advantageous for many sensing applications. At low temperatures, excitation of a highly cycling transition provides a convenient route to high-fidelity readout, allowing for single-shot readout and quantum non-demolition measurements of the electron spin, with fidelities reaching 94.6%[173,176,177]. A key challenge is the extraction and detection of these photons from materials with high refractive indices.

This problem can be overcome by the micromachining the solid-state host[178] and coupling to photonic structures[179–182].

Room-temperature readout typically relies on some spin-projection-dependent change in emitter brightness (for example, spin-dependent inter-system crossings competing with radiative relaxation). Readout contrasts in this scheme can vary significantly, from ≈30% in NV$^-$ centres in diamond[183] to <1% for the nitrogen-vacancy in silicon carbide (NV$_{\mathrm{SiC}}$) defect[172], depending on the relative radiative and non-radiative relaxation rates. Strategies have been developed to further improve readout fidelity in these systems, for example, using spin-dependent ionization to increase contrast[184] and repetitive readout schemes using nuclear spins as ancilla states[185]. Reference[186] reviews several of these strategies for improving readout efficiency.

Electrical manipulation of point defects has been demonstrated in several systems. Spin-to-charge detection has been realized in NV$^-$ centres in diamond[187], Si vacancies in SiC (REF.[188]) and Er^{3+} ions[161]. Electric fields can also be used to modulate the optical properties of defects; Stark tuning of NV$^-$ centres in diamonds can mitigate the effect of spectral diffusion[189], whereas DC bias fields in SiC can be used to deplete nearby charge traps to stabilize the optical transition[190]. Another approach to qubit control focuses on using mechanical resonances to drive transitions between states[191]; acoustically driven strain has been used to manipulate spins in NV$^-$ centres[192] in diamond and divacancy centres in SiC (REF.[193]). Control schemes for optically addressable defects are reviewed in more detail in REF.[194].

Stark tuning
Electric fields can be used to tune the optical transition frequencies of colour centres, usually by inducing a linear shift in frequency with applied field.

Material systems

Although an exhaustive cataloguing of optically active defects in solid-state systems is beyond the scope of this Review, several well-studied systems serve as examples of key concepts and design principles for various applications. A more detailed discussion may be found in REFS[195–198].

Diamond. Diamond has proven to be one of the most successful host materials for optically addressable quantum defects. The most-studied defect in diamond is the NV$^-$ centre, which has been widely explored as a sensor[199–201], quantum register[162,164,165] and quantum communication node[2]. The room-temperature operation, biocompatibility and photostability of the NV$^-$ centre make it an excellent sensor in a wide range of environments. However, the NV$^-$ centre faces several challenges in other quantum applications. It suffers from significant spectral diffusion of its optical transition[202], limited emission into its zero-phonon line (ZPL)[182] and operates in a wavelength range that is not directly compatible with long-distance photon propagation, motivating broad searches for alternative defects. Nevertheless, the NV$^-$ centre remains best-in-class for spin coherence times, with T_{2DD} times surpassing 1 s at low temperature[175]. This coherence time can be extended by mapping the electron spin coherence to a nuclear spin coherence of a nearby ^{13}C, enabling repetitive readout protocols[185] and coherence times of seconds at room temperature[203].

The negatively charged silicon vacancy centre (SiV$^-$) has several desirable optical properties for quantum communication applications (limited spectral diffusion, high Debye–Waller factor[204]) but requires cooling to millikelvin temperatures to overcome phonon-induced dephasing. At 4 K, the spin coherence is 35 ns (REF.[205]), whereas at 10 mK, it can be extended by dynamical decoupling to 10 ms (REF.[176]). These properties have enabled demonstrations of spin–photon entanglement using SiV$^-$ in nanophotonic structures[206,207]. Nearby nuclear spins can be used as ancilla qubits with coherence times of up to 0.2 s (REF.[206]). The spin coherence can also be extended by increasing the energy splitting between spin–orbit states, for example by applying strain[208]. Other negatively charged group IV vacancy defects have also been studied with the goal of achieving larger spin–orbit splittings[209–212] and longer spin coherence times outside the millikelvin range[211,212].

The neutral silicon vacancy (SiV^0) has also been demonstrated as a promising alternative to the NV$^-$ centre, combining many of the desirable optical properties of SiV$^-$, with long spin coherence times possible in the NV$^-$ centre[213–215]. This alternative charge state can be accessed by controlling the Fermi level of diamond[213]. SiV^0 exhibits a spin coherence time of 255 ms with dynamical decoupling at 15 K, and near-transform-limited optical linewidths[213]. The wavelength of the SiV^0 ZPL (946 nm) experiences significantly less attenuation in fibres and is compatible with many frequency conversion schemes for telecom C-band wavelength operation[216].

Silicon carbide. Beyond diamond, many other materials are being pursued as potential hosts for optically active defects. Among the most successful of these is perhaps SiC. SiC shares many of the desirable materials properties of diamond (large bandgap, low background magnetic noise, low spin–orbit coupling) and has the substantial benefit of wafer-scale processing and complementary metal–oxide–semiconductor (CMOS)-processing compatibility[217]. SiC is known to host many defects, and, here, we restrict ourselves to only a small subset of these. A fuller description of the defects hosted by SiC is given in REFS[218,219].

Several defects in SiC have shown promise for quantum communication applications. Long spin coherence times (>1 ms) and spin-dependent fluorescence have been demonstrated in both the neutral divacancy and silicon vacancy in SiC at cryogenic (4–20 K) temperatures[174,220]. As with diamond, nearby nuclei may serve as ancilla qubits for these systems. This has been demonstrated for both silicon vacancies in silicon carbide (SiV$_{\mathrm{SiC}}$)[174] and neutral divacancy defects[221] using a proximal ^{29}Si nucleus. The SiV$_{\mathrm{SiC}}$ defect has also been shown to operate at room temperature, with spin coherence times in the hundreds of microseconds range, comparable to NV$^-$ centres in diamond[172]. However, the contrast from off-resonant excitation is on the order of a half a percent, rather than the 30% achievable with NV$^-$ centres in diamond.

The emission wavelengths of these defects fall in the near-infrared range, making them more amenable to frequency-conversion to telecom wavelengths for quantum communication applications. SiC also plays host to a number of defects that operate directly in the near-infrared range. The NV_{SiC} centre and V^{4+} defect operate near the telecom O-band (1,300 nm)[222,223]. The minimal transmission loss in optical fibres in this range makes these defects promising candidates for quantum communication applications.

SiC as a platform has the additional advantage of mature, CMOS-compatible (nano)fabrication techniques. These nanofabrication procedures enabled several realizations of several interesting control schemes. Purcell-enhanced emission from defects in SiC (REFS[217,224]) using nanophotonic structures, unique spectral shaping via energy-level modulation[225] and acoustic control of the spin degree of freedom[193] have all been demonstrated in SiC.

Rare-earth ion systems. REIs in solid-state hosts present a subtly different class of quantum defects. Transitions present in the free ion are perturbed by the crystal-field interaction with the host, but retain many of their 'atomic' properties, and, in some cases, the optical coherence time is sufficiently long to allow the optical states to be used as qubit states directly. Bulk REI samples have been studied extensively as potential ensemble quantum memories using photon echoes and other techniques[226], including inside nanophotonic structures[227].

Integration of nanophotonic structures with REI-doped crystals has enabled single-ion optical detection and manipulation[179,228], and key requirements for a quantum node have been demonstrated in single erbium ions, including single-shot readout[177]. An alternative approach is to use dipole-allowed transitions to 5*d* orbitals, which are significantly brighter than intra-4*f* transitions, and have been used to both initialize and read out the spin degree of freedom in Ce^{3+} (REF.[229]).

One significant challenge in the use of REIs as quantum resources is the spin coherence time, which is often limited by other REI defects present in the crystal, or host nuclear spins[230]. This motivates the search for new host materials not only for REIs[231] but for all types of quantum defects. REIs have the advantage that the optical and spin properties of the defect resemble those of the implanted ion, rather than a complex combination of implanted ion and vacant site. This has enabled high conversion efficiency (approaching 90%) of ions implanted in host materials[231,232], an important property for generating scalable arrays of these defects.

Prospects for new defects and new material systems. The primary function of the host material is to act as a structural matrix for the defect. A key requirement of a good host is that it introduces minimal additional noise into the system. Though there may be application-specific host requirements (for example, environmental compatibility considerations for sensors) and various strategies to extend coherence times, the generally desirable properties of the host may be summarized as:

1. Bandgap sufficient to support the defect optical transition.
2. Minimal magnetic noise background: low paramagnetic defect concentration, low nuclear spin background. The latter consideration limits the possible materials to those comprised entirely of elements with only nuclear-spin-zero isotopes. Note that this requirement is general to all of the systems described here; magnetic noise from proximal spins is generally undesirable.
3. High Debye temperature and/or low spin–orbit coupling to minimize relaxation and dephasing.

The identification of promising host materials is challenging because of the overwhelming vastness of the chemical space that may meet these basic criteria. The advent of large-scale materials properties repositories, however, has enabled efficient automated searches for new host materials[233].

The optimal properties of a defect are typically application-specific (such as the optimal wavelength operation or the importance of room-temperature operation), though long spin coherence times, optical initialization and spin-dependent emission are generally desirable in all applications[197]. An a priori prediction of the optical and spin properties of defects in solid-state systems represents an outstanding challenge in the field.

In addition to searching for new defects and new host systems, realizing existing bulk systems as nanoparticles would enable several new applications. For example, the use of these systems for in situ sensing, such as NV^- centres in nanodiamonds incorporated into living cells[201], presents an exciting frontier. This mode of operation is unique to optically addressable quantum defects among the systems discussed in this Review; optical addressing enables non-contact probing (unlike in gate-defined structures). Arranging nanoparticles into regular arrays circumvents problems arising from the probabilistic formation of defects from ion implantation into bulk crystals, enabling new implementations of spatially resolved sensing[234]. However, the synthetic methods for creating nanoparticles often introduces additional paramagnetic impurities [235], which has motivated the development of various methods for nanoparticle fabrication, including ball-milling bulk substrates[236], to nanofabrication[237], to wet-chemistry methods[238] and plasma etching of high-purity bulk material[239]. In addition to decoherence from paramagnetic impurities in the nanoparticle, the perennial challenge of maintaining useful optical and spin coherence properties of a defect near a surface is brought into sharp relief in the case of nanoparticles because of their larger surface-to-volume ratio[240,241].

Applications

Quantum sensing. Optically addressable quantum defects have been used extensively in quantum sensing. The key advantages are the contact-free mode of operation (requiring only an optically transparent environment) and the high spatial resolution offered by their point-like nature. Additionally, room-temperature coherence and straightforward integration into nanoparticles make these qubits especially attractive as in situ sensors.

One natural application of these defects is as magnetometers, reviewed extensively in REF.[242]. DC vector magnetometry has been demonstrated with sensitivities of $500\,\mathrm{nT}/\sqrt{\mathrm{Hz}}$ using single NV^- centres in diamond[243] and 50 pT/$\sqrt{\text{Hz}}$ in ensemble samples[244]. Colour centres have also shown great utility sensing AC magnetic fields, achieving sensitivities[245] of 4.3 nT/$\sqrt{\text{Hz}}$, limited by the coherence time of the defect. Further improvements in sensitivity have been demonstrated using quantum logic[168,185] and spin-to-charge readout[184]. Sensitivity to small fields is not the only important metric for AC magnetometers; frequency resolution and precision are also key parameters. Pulse sequences have been developed to enhance the frequency resolution beyond limits imposed by NV$^-$ spin decoherence, and have achieved <100 μHz frequency resolution and <μT precision[4,169], offering a route to single-molecule chemical-shift nuclear magnetic resonance experiments[3]. Combining NV-containing nanodiamonds with scanning probe microscopes enables nanometre-scale imaging[246]. An alternative approach is to construct atomic force microscope cantilevers directly from diamonds containing colour centres[247,248].

Beyond magnetic field sensing, the high thermal conductivities of diamond and SiC have led to their use as nanoscale temperature sensors. Both microwave-assisted and all-optical thermometry schemes with NV$^-$ centres have been demonstrated[201,249], whereas optical thermometry schemes with the silicon-vacancy defects in diamond[250] and SiC[251] have been reported with sensitivities down to 100 mK/$\sqrt{\text{Hz}}$. These schemes rely on subtle changes in the host lattice with temperature, and, so, do not require any additional labelling. Note that these defects all operate in distinct wavelength ranges; optical multiplexing could be used to increase the sensitivity further.

A key challenge remaining in the use of quantum defects as nanoscale sensors is gaining control over the surface of the sensor. Both sensitivity and resolution require that the defect must be close to the sensing target, which necessitates being near the host surface. This requirement brings significant materials engineering challenges; surface-related defects such as charge traps and dangling bonds can lead to Fermi-level pinning and magnetic noise, degrading charge stability and coherence time of near-surface quantum defects. Many research groups have observed that NV$^-$ coherence degrades as NV$^-$ centres are brought closer to the surface[252–254]. Other work has led to the realization of NV$^-$ centres with dynamically decoupled coherence times exceeding 100 μs within nanometres of the surface by careful control over the diamond surface[253,254].

Quantum simulation. The straightforward initialization and control of quantum defects suggests that they may find a natural home in quantum simulation applications. However, the probabilistic nature of formation of these defects makes the construction of a target Hamiltonian extremely challenging. This stands in contrast to lithographically defined qubits (as discussed earlier), where the coupling between qubits can be tuned by applying voltages to gate electrodes. An additional challenge is the length scale of spin–spin interactions (several nanometres) and the minimum defect separation imposed by the optical diffraction limit (hundreds of nanometres), though this challenge may be overcome with spectrally distinct emitters[177].

Instead, several proposals have focused on using nearby spins to serve as a simulator, with the optically active defect serving as a route to both manipulating and reporting on these proximal spins. Proposed systems include using dipolar interactions between nitrogen spins in the bulk as buses[255], exploiting nearby spins at a diamond surface to probe many-body localization[256] and patterning nuclear spins on a surface to realize effects such as frustrated magnetism[257]. A key technical achievement to this end has been the mapping out of the locations of nearby ^{13}C spins in diamond and using this information to manipulate individual nuclear spins[165,258].

Quantum defects find broader applicability when, instead of simulating arbitrary target systems, they are used to probe new physics in disordered systems. One example of this approach is the experimental realization of time crystals using NV$^-$ centres in diamond[259].

Quantum computation. Many of the DiVincenzo criteria have been robustly met in quantum defect systems: optical pumping provides high-fidelity initialization[176,177,205], long spin coherence times have been demonstrated in many systems[176,213,220,258], spin-selective transitions provide a straightforward readout channel and two-qubit gates have been demonstrated using nearby nuclear spins[260]. As with simulation applications, however, the scalability of these systems is hampered by the probabilistic formation of defects and the positions of the nuclear spins surrounding them.

Though these defects may not be suited to large-scale quantum computation, the use of smaller quantum registers[162] may be advantageous in modular quantum computing, enhanced sensing or high-fidelity quantum communication. A key advance to this end is the development of protocols enabling the manipulation of nearby nuclear spins via hyperfine interactions with NV$^-$ centres, enabling registers with tens of qubits[165,258].

Quantum networks. The ability to serve as a spin–photon interface makes quantum defects uniquely well suited for quantum communication applications. The spin degree of freedom can serve as a local quantum memory, whereas the photon takes the role of a flying qubit. Remote entanglement over the kilometre scale has already been demonstrated with defects in diamond[2].

A common scheme used to generate entanglement between two defects uses the interference of indistinguishable photons on a beam splitter. An optimal defect for this application would have a high rate of generation of indistinguishable photons, and these photons would experience minimal loss over the distance they propagate. Though NV$^-$ centres in diamond have been the main platform used to demonstrate these entanglement experiments[2,261], the large fraction of the emission (>0.97) into the phonon sideband[182], spectral diffusion of the optical transitions and the high attenuation of 637-nm light through fibres on the kilometre scale precludes the 'as is' use of NV$^-$ centres in a large quantum network. Efforts to address this issue include nanophotonic structures to enhance the ZPL emission[181,182] and frequency conversion to telecom wavelengths[262].

Other quantum defects have been proposed as alternatives to NV⁻ centres. SiV⁻ and SiV⁰ show reduced spectral diffusion because of their inversion symmetric structures[213,263], allowing for higher entanglement generation rates. Silicon vacancies in SiC have also shown limited spectral diffusion[174] (in this case, it is the similarity between permanent electric dipole moments in the ground and excited states that minimizes spectral diffusion).

Several key technical accomplishments for quantum communication have been demonstrated with the SiV⁻ defect. Cavity-mediated interactions between different defects have been demonstrated[264,265], as have spin–photon interfaces and the formation of local quantum registers[206,207]. However, the limited spin coherence time and millikelvin operation temperature of SiV⁻ is a significant challenge for building a large network. This has motivated two distinct approaches to improving this system; increasing the ground-state splitting to enable higher-temperature operation by using heavier elements and engineering a spin-1 analogue of SiV⁻. The former approach has yielded germanium-vacancy, tin-vacancy and lead-vacancy defects[209–212], with $T_2^* = 540$ ns observed for the SnV centre at 2.9 (REF.[212]). The latter approach has yielded the SiV⁰ defect, with a dynamically decoupled coherence time of 255 ms at <15 K (REF.[213]), and in which spin-dependent fluorescence has recently been demonstrated[266].

One major frontier in this field is the integration of quantum defects into nanophotonic cavities to enhance the atom–photon interaction. Significant effort has been dedicated to integrating NV⁻ centres into nanophotonic structures[182]; however, the sensitivity of the optical transition to fluctuating charges precludes high cooperativity in such structures[202,267]. Because of their larger spectral stability, SiV⁻ centres implanted into diamond nanobeam cavities have achieved cooperativity of >100 (REF.[268]). Future work along this direction would benefit significantly from a material system that allows for high-quality heteroepitaxial growth, such as SiC (REF.[217]).

Ultimately, for long-range quantum communication, operation in the telecom band is essential. Although there is an active subfield working on realizing low-noise, high-efficiency, quantum frequency conversion to the telecom band for various emitters, it would undoubtedly be beneficial to have a quantum defect that emits directly in the telecom band. Er^{3+} ions are one of the few systems that have optical transitions in the C-band (1,550-nm region). Detection of single ions has been historically limited by the slow emission rate (≈100 Hz); however, integrated nanophotonic cavities have demonstrated that significant Purcell-enhanced emission rates can be achieved[177,179], presenting a route towards long-range, single-ion, Er^{3+}-based quantum repeaters. Several defects in SiC, such as the NV centre and V^{4+} defect, lie within the only slightly less optimal O-band (1,300-nm region)[222,223].

Summary

Optically addressable quantum defects combine the two capabilities of magnetic resonance and single-molecule fluorescent microscopy, enabling single-spin manipulation and detection, even at room temperature. Devising methods for deterministic formation and placement will enable their use in quantum simulation and computation applications. Furthermore, they present a powerful spin–photon interface for quantum communication applications, and their broad environmental compatibility and single-spin sensitivity makes them extremely versatile and sensitive quantum sensors.

Outlook

In this Review, we have highlighted the variety of quantum systems in which semiconductor qubits can be implemented and the applications they offer. With high-fidelity initialization and readout methods, long coherence times with fast gate operation, inter-qubit coupling and coupling to photons, many of these systems fulfil criteria essential for realizing quantum computation. We envision that a diverse ecosystem of qubits will allow for many different quantum applications, with inherent advantages and trade-offs for each qubit. The semiconductor community is very far from having 'picked a winner'. As this Review has highlighted, a 'winner' may never even need to be picked; rather, the diverse and eclectic nature of semiconductor qubits is likely to remain a defining feature of this platform. This situation is rather different from superconducting qubits, for instance, where the community has mostly converged towards a rather narrow portfolio of implementations, optimized for quantum information processing.

FIGURE 5 illustrates a few applications that are likely to be pursued using the broad palette of semiconductor qubits. Charge–photon and spin–photon interfaces with strong coupling, based on circuit quantum electrodynamics, have recently been demonstrated (and reviewed in REF.[20]), and advances in resonator engineering may lead to light–matter networks (FIG. 5a), entangling distant qubits for a surface code and other qubit–qubit connectivities. A quantum internet (FIG. 5b) based on secure quantum cryptography and entanglement beacons may become possible when semiconductor qubits are made optically active. FIGURE 5c shows a powerful application of gate-controlled spin qubits in QDs, where specific 2D arrays implement Hamiltonians desired for quantum simulations. Dopant atoms with long-lived spin states can be used to store information as quantum memories (FIG. 5d), including in ensembles coupled to microwave cavities or in hybrid donor–dot systems. Quantum sensing applications are already widely researched[269], with nanomechanical piezoelectric actuators used to create scanning quantum probes (FIG. 5e) for magnetism and new spin textures. Lastly, quantum systems operable above millikelvin-scale temperatures would go a long way towards solving the problem of wiring and cooling large numbers of physical qubits; FIG. 5f shows a few semiconductor qubits that have already been operated above dilution-refrigerator temperatures.

Several challenges remain for semiconductor quantum circuits. Probably the most significant one is the establishment of a scalable and reproducible fabrication process. This task is rendered onerous by the extremely small physical dimensions of semiconductor qubits, but the future prospects are brightened by the potential for integration with industry-based manufacturing methods. Calibrating, operating and stabilizing large arrays or simultaneously performing and validating quantum operations over multiple qubits are among the current challenges faced by all quantum computing research groups. The broad issues are superficially similar to those in superconducting circuits and trapped ions, but the small size of semiconductor qubits poses unique problems with crosstalk and placement of classical readout devices. In return, the extreme density afforded by semiconductor systems lends credibility to the prospect of integrating hundreds of millions of qubits on a chip, as necessary for the most useful quantum algorithms integrated with quantum error correction. For quantum sensing, the next frontier is developing methods to operate in 3D and under an ever wider range of environmental conditions.

In conclusion, the diversity and flexibility afforded by semiconductor materials and qubit encodings will continue to encourage the community to work in many complementary directions. An increasing engagement with the semiconductor industry will enable exceptional levels of qubit density and device reliability; this will not only enable the production of useful and manufacturable quantum devices but also continue to expand the scope for studying fundamental science in engineered quantum systems of unprecedented complexity.

1. DiVincenzo, D. The physical implementation of quantum computation. *Fortschr. Phys.* **48**, 771–783 (2008).
2. Hensen, B. et al. Loophole-free Bell inequality violation using electron spins separated by 1.3 kilometres. *Nature* **526**, 682–686 (2015).
3. Aslam, N. et al. Nanoscale nuclear magnetic resonance with chemical resolution. *Science* **357**, 67–71 (2017).
4. Boss, J. M., Cujia, K. S., Zopes, J. & Degen, C. L. Quantum sensing with arbitrary frequency resolution. *Science* **356**, 837–840 (2017).
5. Michler, P. *Quantum Dots for Quantum Information Technologies* (Springer, 2017).
6. Kjaergaard, M. et al. Superconducting qubits: Current state of play. *Annu. Rev. Condens. Matter Phys.* **11**, 369–395 (2020).
7. Lutchyn, R. M. et al. Majorana zero modes in superconductor–semiconductor heterostructures. *Nat. Rev. Mater.* **3**, 52–68 (2018).
8. Reed, M. et al. Observation of discrete electronic states in a zero-dimensional semiconductor nanostructure. *Phys. Rev. Lett.* **60**, 535–537 (1988).
9. Elzerman, J. M. et al. Few-electron quantum dot circuit with integrated charge read out. *Phys. Rev. B* **67**, 161308 (2003).
10. Hayashi, T., Fujisawa, T., Cheong, H. D., Jeong, Y. H. & Hirayama, Y. Coherent manipulation of electronic states in a double quantum dot. *Phys. Rev. Lett.* **91**, 226804 (2003).
11. Petersson, K. D., Petta, J. R., Lu, H. & Gossard, A. C. Quantum coherence in a one-electron semiconductor charge qubit. *Phys. Rev. Lett.* **105**, 246804 (2010).
12. Cao, G. et al. Ultrafast universal quantum control of a quantum-dot charge qubit using Landau–Zener–Stückelberg interference. *Nat. Commun.* **4**, 1401 (2013).
13. Schoenfield, J. S., Freeman, B. M. & Jiang, H. Coherent manipulation of valley states at multiple charge configurations of a silicon quantum dot device. *Nat. Commun.* **8**, 64 (2017).
14. Penthorn, N. E., Schoenfield, J. S., Rooney, J. D., Edge, L. F. & Jiang, H. Two-axis quantum control of a fast valley qubit in silicon. *Npj Quantum Inf.* **5**, 94 (2019).
15. Mi, X., Cady, J. V., Zajac, D. M., Deelman, P. W. & Petta, J. R. Strong coupling of a single electron in silicon to a microwave photon. *Science* **355**, 156–158 (2017).
16. Scarlino, P. et al. Coherent microwave-photon-mediated coupling between a semiconductor and a superconducting qubit. *Nat. Commun.* **10**, 3011 (2019).
17. Mi, X. et al. A coherent spin–photon interface in silicon. *Nature* **555**, 599–603 (2018).
18. Samkharadze, N. et al. Strong spin-photon coupling in silicon. *Science* **359**, 1123–1127 (2018).
19. Landig, A. et al. Coherent spin–photon coupling using a resonant exchange qubit. *Nature* **560**, 179–184 (2018).
20. Burkard, G., Gullans, M. J., Mi, X. & Petta, J. R. Superconductor–semiconductor hybrid-circuit quantum electrodynamics. *Nat. Rev. Phys.* **2**, 129–140 (2020).
21. Loss, D. & DiVincenzo, D. Quantum computation with quantum dots. *Phys. Rev. A* **57**, 120–126 (1998).
22. Yang, C. H. et al. Operation of a silicon quantum processor unit cell above one kelvin. *Nature* **580**, 350–354 (2020).
23. Petit, L. et al. Universal quantum logic in hot silicon qubits. *Nature* **580**, 355–359 (2020).
24. Veldhorst, M. et al. An addressable quantum dot qubit with fault-tolerant control-fidelity. *Nature* **9**, 981–985 (2014).
25. Yoneda, J. et al. A quantum-dot spin qubit with coherence limited by charge noise and fidelity higher than 99.9%. *Nat. Nanotechnol.* **13**, 102–106 (2018).
26. Koppens, F. et al. Driven coherent oscillations of a single electron spin in a quantum dot. *Nature* **442**, 766–771 (2006).
27. Brunner, R. et al. Two-qubit gate of combined single-spin rotation and interdot spin exchange in a double quantum dot. *Phys. Rev. Lett.* **107**, 146801 (2011).
28. Veldhorst, M. et al. A two-qubit logic gate in silicon. *Nature* **526**, 410–414 (2015).
29. West, A. et al. Gate-based single-shot readout of spins in silicon. *Nat. Nanotechnol.* **14**, 437–441 (2019).
30. Higginbotham, A. P., Kuemmeth, F., Hanson, M. P., Gossard, A. C. & Marcus, C. M. Coherent operations and screening in multielectron spin qubits. *Phys. Rev. Lett.* **112**, 026801 (2014).
31. Leon, R. C. C. et al. Coherent spin control of s-, p-, d- and f-electrons in a silicon quantum dot. *Nat. Commun.* **11**, 797 (2020).
32. Mehl, S. & DiVincenzo, D. P. Noise-protected gate for six-electron double-dot qubit. *Phys. Rev. B* **88**, 161408 (2013).
33. Malinowski, F. et al. Fast spin exchange across a multielectron mediator. *Nat. Commun.* **10**, 1196 (2019).
34. Petta, J. et al. Coherent manipulation of coupled electron spins in semiconductor quantum dots. *Science* **309**, 2180–2184 (2005).
35. Levy, J. Universal quantum computation with spin-1/2 pairs and heisenberg exchange. *Phys. Rev. Lett.* **89**, 147902 (2002).
36. Benjamin, S. C. Simple pulses for universal quantum computation with a Heisenberg ABAB chain. *Phys. Rev. A* **64**, 054303 (2001).
37. Foletti, S., Bluhm, H., Mahalu, D., Umansky, V. & Yacoby, A. Universal quantum control of two-electron spin quantum bits using dynamic nuclear polarization. *Nat. Phy.* **5**, 903–908 (2009).
38. Reed, M. D. et al. Reduced sensitivity to charge noise in semiconductor spin qubits via symmetric operation. *Phys. Rev. Lett.* **116**, 110402 (2016).
39. Martins, F. et al. Noise suppression using symmetric exchange gates in spin qubits. *Phys. Rev. Lett.* **116**, 116801 (2016).
40. Bertrand, B. et al. Quantum manipulation of two-electron spin states in isolated double quantum dots. *Phys. Rev. Lett.* **115**, 096801 (2015).
41. Kornich, V., Kloeffel, C. & Loss, D. Phonon-mediated decay of singlet-triplet qubits in double quantum dots. *Phys. Rev. B* **89**, 085410 (2014).
42. Medford, J. et al. Self-consistent measurement and state tomography of an exchange-only spin qubit. *Nat. Nanotechnol.* **8**, 654–659 (2013).
43. Eng, K. et al. Isotopically enhanced triple-quantum-dot qubit. *Sci. Adv.* **1**, e1500214 (2015).
44. DiVincenzo, D., Bacon, C., Kempe, J., Burkard, G. & Whaley, K. Universal quantum computation with the exchange interaction. *Nature* **408**, 339–342 (2000).
45. Malinowski, F. K. et al. Symmetric operation of the resonant exchange qubit. *Phys. Rev. B* **96**, 045443 (2017).
46. Russ, M. & Burkard, G. Three-electron spin qubits. *J. Phys. Condens. Matter* **29**, 393001 (2017).
47. Kim, D. et al. Quantum control and process tomography of a semiconductor quantum dot hybrid qubit. *Nature* **511**, 70–74 (2014).
48. Russ, M., Petta, J. R. & Burkard, G. Quadrupolar exchange-only spin qubit. *Phys. Rev. Lett.* **121**, 177701 (2018).
49. Sala, A., Qvist, J. H. & Danon, J. Highly tunable exchange-only singlet-only qubit in a GaAs triple quantum dot. *Phys. Rev. Res.* **2**, 012062 (2020).
50. Vukušić, L., Kukučka, J., Watzinger, H. & Katsaros, G. Fast hole tunneling times in germanium hut wires probed by single-shot reflectometry. *Nano Lett.* **17**, 5706 (2017).
51. Maurand, R. et al. A CMOS silicon spin qubit. *Nat. Commun.* **7**, 13575 (2016).
52. Hendrickx, N. W., Franke, D. P., Sammak, A., Scappucci, G. & Veldhorst, M. Fast two-qubit logic with holes in germanium. *Nature* **577**, 487–491 (2020).
53. Scappucci, G. et al. The germanium quantum information route. *Nat. Rev. Mater.* https://doi.org/10.1038/s41578-020-00262-z (2020).
54. Camenzind, L. C. et al. Hyperfine-phonon spin relaxation in a single-electron GaAs quantum dot. *Nat. Commun.* **9**, 3454 (2018).
55. Yoneda, J. et al. Quantum non-demolition readout of an electron spin in silicon. *Nat. Commun.* **11**, 1144 (2020).
56. Elzerman, J. et al. Single-shot read-out of an individual electron spin in a quantum dot. *Nature* **430**, 431–435 (2004).
57. Petersson, K. et al. Charge and spin state readout of a double quantum dot coupled to a resonator. *Nano Lett.* **10**, 2789–2793 (2010).
58. Barthel, C., Reilly, D., Marcus, C., Hanson, M. & Gossard, A. Rapid single-shot measurement of a singlet-triplet qubit. *Phys. Rev. Lett.* **103**, 160503 (2009).
59. Zheng, G. et al. Rapid gate-based spin read-out in silicon using an on-chip resonator. *Nat. Nanotechnol.* **14**, 742–746 (2019).
60. Gonzalez-Zalba, M., Barraud, S., Ferguson, A. & Betz, A. Probing the limits of gate-based charge sensing. *Nat. Commun.* **6**, 6084 (2015).
61. Ono, K., Austing, D. G., Tokura, Y. & Tarucha, S. Current rectification by Pauli exclusion in a weakly coupled double quantum dot system. *Science* **297**, 156–158 (2002).
62. Reilly, D., Marcus, C., Hanson, M. & Gossard, A. Fast single-charge sensing with a rf quantum point contact. *Appl. Phys. Lett.* **91**, 162101 (2007).
63. Crippa, A. et al. Gate-reflectometry dispersive readout and coherent control of a spin qubit in silicon. *Nat. Commun.* **10**, 2776 (2019).
64. Urdampilleta, M. et al. Gate-based high fidelity spin readout in a cmos device. *Nat. Nanotechnol.* **14**, 737–741 (2019).
65. Harvey-Collard, P. et al. High-fidelity single-shot readout for a spin qubit via an enhanced latching mechanism. *Phys. Rev. X* **8**, 021046 (2018).
66. Pla, J. J. et al. High-fidelity readout and control of a nuclear spin qubit in silicon. *Nature* **496**, 334–338 (2013).

67. Watson, T. F., Weber, B., House, M. G., Büch, H. & Simmons, M. Y. High-fidelity rapid initialization and read-out of an electron spin via the single donor D^- charge state. *Phys. Rev. Lett.* **115**, 166806 (2015).
68. Nowack, K. C., Koppens, F., Nazarov, Y. V. & Vandersypen, L. Coherent control of a single electron spin with electric fields. *Science* **318**, 1430–1433 (2007).
69. Nadj-Perge, S., Frolov, S., Bakkers, E. & Kouwenhoven, L. Spin–orbit qubit in a semiconductor nanowire. *Nature* **468**, 1084–1087 (2010).
70. Corna, A. et al. Electrically driven electron spin resonance mediated by spin–valley–orbit coupling in a silicon quantum dot. *Npj Quantum Inf.* **4**, 6 (2018).
71. Crippa, A. et al. Electrical spin driving by *g*-matrix modulation in spin-orbit qubits. *Phys. Rev. Lett.* **120**, 137702 (2018).
72. Golovach, V. N., Borhani, M. & Loss, D. Electric-dipole-induced spin resonance in quantum dots. *Phys. Rev. B* **74**, 165319 (2006).
73. Pioro-Ladriere, M. et al. Electrically driven single-electron spin resonance in a slanting Zeeman field. *Nat. Phys.* **4**, 776–779 (2008).
74. Kawakami, E. et al. Electrical control of a long-lived spin qubit in a Si/SiGe quantum dot. *Nat. Nanotechnol.* **9**, 666–670 (2014).
75. Zajac, D. et al. Resonantly driven CNOT gate for electron spins. *Science* **359**, 439–442 (2018).
76. Malinowski, F. et al. Notch filtering the nuclear environment of a spin qubit. *Nat. Nanotechnol.* **12**, 16–20 (2017).
77. Cerfontaine, P. et al. Closed-loop control of a GaAs-based singlet-triplet spin qubit with 99.5% gate fidelity and low leakage. *Nature* **11**, 4144 (2020).
78. Mortemousque, P. et al. Coherent control of individual electron spins in a two dimensional array of quantum dots. *Nat. Nanotechnol.* https://doi.org/10.1038/s41565-020-00816-w (2020).
79. Qiao, H. et al. Coherent multispin exchange coupling in a quantum-dot spin chain. *Phys. Rev. X* **10**, 031006 (2020).
80. Kandel, Y. P. et al. Coherent spin-state transfer via Heisenberg exchange. *Nature* **573**, 553–557 (2019).
81. Dehollain, J. P. et al. Nagaoka ferromagnetism observed in a quantum dot plaquette. *Nature* **579**, 528–533 (2020).
82. Pla, J. J. et al. A single-atom electron spin qubit in silicon. *Nature* **489**, 541–545 (2012).
83. Maune, B. M. et al. Coherent singlet-triplet oscillations in a silicon-based double quantum dot. *Nature* **481**, 344–347 (2012).
84. Ansaloni, F. et al. Single-electron control in a foundry-fabricated two-dimensional qubit array. *Nat Commun.* **11**, 6399 (2020).
85. Zajac, D., Hazard, T., Mi, X., Nielsen, E. & Petta, J. Scalable gate architecture for a one-dimensional array of semiconductor spin qubits. *Phys. Rev. Appl.* **6**, 054013 (2016).
86. Itoh, K. M. & Watanabe, H. Isotope engineering of silicon and diamond for quantum computing and sensing applications. *MRS Commun.* **4**, 143–157 (2014).
87. Zwanenburg, F. A. et al. Silicon quantum electronics. *Rev. Mod. Phys.* **85**, 961 (2013).
88. Watzinger, H. et al. A germanium hole spin qubit. *Nat. Commun.* **9**, 3902 (2018).
89. Malinowski, F. K. et al. Spectrum of the nuclear environment for GaAs spin qubits. *Phys. Rev. Lett.* **118**, 177702 (2017).
90. Tahan, C. Democratizing spin qubits. Preprint at *arXiv* 2001.08251 (2020).
91. Hoffman, S., Schrade, C., Klinovaja, J. & Loss, D. Universal quantum computation with hybrid spin-Majorana qubits. *Phys. Rev. B* **94**, 045316 (2016).
92. Hensgens, T. et al. Quantum simulation of a Fermi–Hubbard model using a semiconductor quantum dot array. *Nature* **548**, 70–73 (2017).
93. Veldhorst, M., Eenink, H., Yang, C. & Dzurak, A. Silicon CMOS architecture for a spin-based quantum computer. *Nat. Commun.* **8**, 1766 (2017).
94. Vandersypen, L. et al. Interfacing spin qubits in quantum dots and donors—hot, dense, and coherent. *Npj Quantum Inf.* **3**, 34 (2017).
95. Watson, T. et al. A programmable two-qubit quantum processor in silicon. *Nature* **555**, 633–637 (2018).
96. Bertrand, B. et al. Fast spin information transfer between distant quantum dots using individual electrons. *Nat. Nanotechnol.* **11**, 672–676 (2016).
97. Mills, A. et al. Shuttling a single charge across a one-dimensional array of silicon quantum dots. *Nat. Commun.* **10**, 1063 (2019).
98. Trif, M., Golovach, V. N. & Loss, D. Spin dynamics in InAs nanowire quantum dots coupled to a transmission line. *Phys. Rev. B* **77**, 045434 (2008).
99. Borjans, F., Croot, X. G., Mi, X., Gullans, M. J. & Petta, J. R. Resonant microwave-mediated interactions between distant electron spins. *Nature* **577**, 195–198 (2020).
100. Kohn, W. & Luttinger, J. Theory of donor states in silicon. *Phys. Rev.* **98**, 915 (1955).
101. Feher, G. & Gere, E. Electron spin resonance experiments on donors in silicon. II. Electron spin relaxation effects. *Phys. Rev.* **114**, 1245 (1959).
102. Kane, B. E. A silicon-based nuclear spin quantum computer. *Nature* **393**, 133–137 (1998).
103. Tyryshkin, A. et al. Coherence of spin qubits in silicon. *J. Phys. Condens. Matter* **18**, S783 (2006).
104. Tyryshkin, A. M. et al. Electron spin coherence exceeding seconds in high-purity silicon. *Nat. Mater.* **11**, 143–147 (2012).
105. Morse, K. J. et al. Zero-field optical magnetic resonance study of phosphorus donors in 28-silicon. *Phys. Rev. B* **97**, 115205 (2018).
106. Ma, W.-L., Wolfowicz, G., Li, S.-S., Morton, J. J. L. & Liu, R.-B. Classical nature of nuclear spin noise near clock transitions of bi donors in silicon. *Phys. Rev. B* **92**, 161403 (2015).
107. Witzel, W., Hu, X. & Sarma, S. D. Decoherence induced by anisotropic hyperfine interaction in Si spin qubits. *Phys. Rev. B* **76**, 035212 (2007).
108. Morton, J. J. et al. Solid-state quantum memory using the ^{31}P nuclear spin. *Nature* **455**, 1085–1088 (2008).
109. Simmons, S. et al. Entanglement in a solid-state spin ensemble. *Nature* **470**, 69–72 (2011).
110. Steger, M. et al. Quantum information storage for over 180 s using donor spins in a 28Si "semiconductor vacuum". *Science* **336**, 1280–1283 (2012).
111. Saeedi, K. et al. Room-temperature quantum bit storage exceeding 39 minutes using ionized donors in silicon-28. *Science* **342**, 830–833 (2013).
112. Bienfait, A. et al. Controlling spin relaxation with a cavity. *Nature* **531**, 74–77 (2016).
113. Fuechsle, M. et al. A single-atom transistor. *Nat. Nanotechnol.* **7**, 242–246 (2012).
114. Jamieson, D. N. et al. Controlled shallow single-ion implantation in silicon using an active substrate for sub-20-keV ions. *Appl. Phys. Lett.* **86**, 202101 (2005).
115. Angus, S. J., Ferguson, A. J., Dzurak, A. S. & Clark, R. G. Gate-defined quantum dots in intrinsic silicon. *Nano Lett.* **7**, 2051–2055 (2007).
116. Morello, A. et al. Single-shot readout of an electron spin in silicon. *Nature* **467**, 687–691 (2010).
117. Büch, H., Mahapatra, S., Rahman, R., Morello, A. & Simmons, M. Spin readout and addressability of phosphorus-donor clusters in silicon. *Nat. Commun.* **4**, 2017 (2013).
118. Keith, D. et al. Single-shot spin readout in semiconductors near the shot-noise sensitivity limit. *Phys. Rev. X* **9**, 041003 (2019).
119. Pakkiam, P. et al. Single-shot single-gate rf spin readout in silicon. *Phys. Rev. X* **8**, 041032 (2018).
120. Tenberg, S. B. et al. Electron spin relaxation of single phosphorus donors in metal-oxide-semiconductor nanoscale devices. *Phys. Rev. B* **99**, 205306 (2019).
121. Watson, T. F. et al. Atomically engineered electron spin lifetimes of 30 s in silicon. *Sci. Adv.* **3**, e1602811 (2017).
122. Gumann, P. et al. NMR study of optically hyperpolarized phosphorus donor nuclei in silicon. *Phys. Rev. B* **98**, 180405 (2018).
123. Dreher, L., Hoehne, F., Stutzmann, M. & Brandt, M. S. Nuclear spins of ionized phosphorus donors in silicon. *Phys. Rev. Lett.* **108**, 027602 (2012).
124. Muhonen, J. T. et al. Storing quantum information for 30 seconds in a nanoelectronic device. *Nat. Nanotechnol.* **9**, 986–991 (2014).
125. Dehollain, J. P. et al. Bell's inequality violation with spins in silicon. *Nat. Nanotechnol.* **11**, 242–246 (2016).
126. Muhonen, J. et al. Quantifying the quantum gate fidelity of single-atom spin qubits in silicon by randomized benchmarking. *J. Phys. Condens. Matter* **27**, 154205 (2015).
127. Dehollain, J. P. et al. Optimization of a solid-state electron spin qubit using gate set tomography. *New J. Phys.* **18**, 103018 (2016).
128. Wolfowicz, G. et al. Atomic clock transitions in silicon-based spin qubits. *Nat. Nanotechnol.* **8**, 561–564 (2013).
129. Asaad, S. et al. Coherent electrical control of a single high-spin nucleus in silicon. *Nature* **579**, 205–209 (2020).
130. Kobayashi, T. Engineering long spin coherence times of spin–orbit qubits in silicon. *Nat. Mater.* **20**, 38–42 (2021).
131. Morello, A., Pla, J. J., Bertet, P. & Jamieson, D. N. Donor spins in silicon for quantum technologies. *Adv. Quantum Technol.* **3**, 2000005 (2020).
132. Franke, D. P. et al. Interaction of strain and nuclear spins in silicon: Quadrupolar effects on ionized donors. *Phys. Rev. Lett.* **115**, 057601 (2015).
133. Zhang, Q. et al. Single rare-earth ions as atomic-scale probes in ultrascaled transistors. *Nano Lett.* **19**, 5025–5030 (2019).
134. Pezzè, L., Smerzi, A., Oberthaler, M. K., Schmied, R. & Treutlein, P. Quantum metrology with nonclassical states of atomic ensembles. *Rev. Mod. Phys.* **90**, 035005 (2018).
135. Matsuzaki, Y., Benjamin, S. C. & Fitzsimons, J. Magnetic field sensing beyond the standard quantum limit under the effect of decoherence. *Phys. Rev. A* **84**, 012103 (2011).
136. Wüst, G. et al. Role of the electron spin in determining the coherence of the nuclear spins in a quantum dot. *Nat. Nanotechnol.* **11**, 885–889 (2016).
137. Delbecq, M. R. et al. Quantum dephasing in a gated GaAs triple quantum dot due to nonergodic noise. *Phys. Rev. Lett.* **116**, 046802 (2016).
138. Mądzik, M. T. et al. Controllable freezing of the nuclear spin bath in a single-atom spin qubit. *Sci. Adv.* **6**, eaba3442 (2020).
139. Salfi, J. et al. Quantum simulation of the Hubbard model with dopant atoms in silicon. *Nat. Commun.* **7**, 11342 (2016).
140. Sieberer, L. M. et al. Digital quantum simulation, Trotter errors, and quantum chaos of the kicked top. *Npj Quantum Inf.* **5**, 78 (2019).
141. Mourik, V. et al. Exploring quantum chaos with a single nuclear spin. *Phys. Rev. E* **98**, 042206 (2018).
142. Dehollain, J. P. et al. Single-shot readout and relaxation of singlet and triplet states in exchange-coupled ^{31}P electron spins in silicon. *Phys. Rev. Lett.* **112**, 236801 (2014).
143. González-Zalba, M. F. et al. An exchange-coupled donor molecule in silicon. *Nano Lett.* **14**, 5672–5676 (2014).
144. He, Y. et al. A two-qubit gate between phosphorus donor electrons in silicon. *Nature* **571**, 371–375 (2019).
145. Kalra, R., Laucht, A., Hill, C. D. & Morello, A. Robust two-qubit gates for donors in silicon controlled by hyperfine interactions. *Phys. Rev. X* **4**, 021044 (2014).
146. Mądzik, M. T. et al. Conditional quantum operation of two exchange-coupled single-donor spin qubits in a MOS-compatible silicon device. *Nat. Commun.* **12**, 181 (2021).
147. Koiller, B., Hu, X. & Sarma, S. D. Exchange in silicon-based quantum computer architecture. *Phys. Rev. Lett.* **88**, 027903 (2001).
148. Srinivasa, V., Xu, H. & Taylor, J. M. Tunable spin-qubit coupling mediated by a multielectron quantum dot. *Phys. Rev. Lett.* **114**, 226803 (2015).
149. Mohiyaddin, F. A. et al. Transport of spin qubits with donor chains under realistic experimental conditions. *Phys. Rev. B* **94**, 045314 (2016).
150. Trifunovic, L., Pedrocchi, F. L. & Loss, D. Long-distance entanglement of spin qubits via ferromagnet. *Phys. Rev. X* **3**, 041023 (2013).
151. Salfi, J., Mol, J. A., Culcer, D. & Rogge, S. Charge-insensitive single-atom spin-orbit qubit in silicon. *Phys. Revi. Lett.* **116**, 246801 (2016).
152. Calderon, M., Koiller, B., Hu, X. & Sarma, S. D. Quantum control of donor electrons at the Si–SiO$_2$ interface. *Phys. Rev. Lett.* **96**, 096802 (2006).
153. Tosi, G. et al. Silicon quantum processor with robust long-distance qubit couplings. *Nat. Commun.* **8**, 450 (2017).
154. Harvey-Collard, P. et al. Coherent coupling between a quantum dot and a donor in silicon. *Nat. Commun.* **8**, 1029 (2017).
155. Hill, C. D. et al. A surface code quantum computer in silicon. *Sci. Adv.* **1**, e1500707 (2015).
156. O'Gorman, J., Nickerson, N. H., Ross, P., Morton, J. J. & Benjamin, S. C. A silicon-based surface code quantum computer. *Npj Quantum Inf.* **2**, 15019 (2016).
157. Pica, G., Lovett, B. W., Bhatt, R. N., Schenkel, T. & Lyon, S. A. Surface code architecture for donors and dots in silicon with imprecise and nonuniform qubit couplings. *Phys. Rev. B* **93**, 035306 (2016).
158. Wesenberg, J. H. et al. Quantum computing with an electron spin ensemble. *Phys. Rev. Lett.* **103**, 070502 (2009).

159. Morse, K. J. et al. A photonic platform for donor spin qubits in silicon. *Sci. Adv.* **3**, e1700930 (2017).
160. Yan, X. et al. A quantum computer architecture based on silicon donor qubits coupled by photons. *Adv. Quantum Technol.* **3**, 2000011 (2020).
161. Yin, C. et al. Optical addressing of an individual erbium ion in silicon. *Nature* **497**, 91–94 (2013).
162. Dutt, M. V. G. et al. Quantum register based on individual electronic and nuclear spin qubits in diamond. *Science* **316**, 1312–1316 (2007).
163. Dolde, F. et al. Room-temperature entanglement between single defect spins in diamond. *Nat. Phys.* **9**, 139–143 (2013).
164. Neumann, P. et al. Quantum register based on coupled electron spins in a room-temperature solid. *Nat. Phys.* **6**, 249–253 (2010).
165. Bradley, C. E. et al. A ten-qubit solid-state spin register with quantum memory up to one minute. *Phys. Rev. X* **9**, 031045 (2019).
166. Maze, J. R. et al. Nanoscale magnetic sensing with an individual electronic spin in diamond. *Nature* **455**, 644–647 (2008).
167. Taylor, J. M. et al. High-sensitivity diamond magnetometer with nanoscale resolution. *Nat. Phys.* **4**, 810–816 (2008).
168. Lovchinsky, I. et al. Nuclear magnetic resonance detection and spectroscopy of single proteins using quantum logic. *Science* **351**, 836–841 (2016).
169. Schmitt, S. et al. Submillihertz magnetic spectroscopy performed with a nanoscale quantum sensor. *Science* **356**, 832–837 (2017).
170. Togan, E. et al. Quantum entanglement between an optical photon and a solid-state spin qubit. *Nature* **466**, 730–734 (2010).
171. Warburton, R. J. Single spins in self-assembled quantum dots. *Nat. Mater.* **12**, 483–493 (2013).
172. Widmann, M. et al. Coherent control of single spins in silicon carbide at room temperature. *Nat. Mater.* **14**, 164–168 (2015).
173. Robledo, L. et al. High-fidelity projective read-out of a solid-state spin quantum register. *Nature* **477**, 574–578 (2011).
174. Nagy, R. et al. High-fidelity spin and optical control of single silicon-vacancy centres in silicon carbide. *Nat. Commun.* **10**, 1954 (2019).
175. Abobeih, M. H. et al. One-second coherence for a single electron spin coupled to a multi-qubit nuclear-spin environment. *Nat. Commun.* **9**, 2552 (2018).
176. Sukachev, D. D. et al. Silicon-vacancy spin qubit in diamond: a quantum memory exceeding 10 ms with single-shot state readout. *Phys. Rev. Lett.* **119**, 223602 (2017).
177. Raha, M. et al. Optical quantum nondemolition measurement of a single rare earth ion qubit. *Nat. Commun.* **11**, 1605 (2020).
178. Hadden, J. P. et al. Strongly enhanced photon collection from diamond defect centers under microfabricated integrated solid immersion lenses. *Appl. Phys. Lett.* **97**, 241901 (2010).
179. Dibos, A. M., Raha, M., Phenicie, C. M. & Thompson, J. D. Atomic source of single photons in the telecom band. *Phys. Rev. Lett.* **120**, 243601 (2018).
180. Hausmann, B. J. M. et al. Integrated diamond networks for quantum nanophotonics. *Nano Lett.* **12**, 1578–1582 (2012).
181. Gould, M. et al. Large-scale GaP-on-diamond integrated photonics platform for NV center-based quantum information. *J. Opt. Soc. Am. B* **33**, B35–B42 (2016).
182. Barclay, P. E., Fu, K.-M. C., Santori, C., Faraon, A. & Beausoleil, R. G. Hybrid nanocavity resonant enhancement of color center emission in diamond. *Phys. Rev. X* **1**, 011007 (2011).
183. Steiner, M., Neumann, P., Beck, J., Jelezko, F. & Wrachtrup, J. Universal enhancement of the optical readout fidelity of single electron spins at nitrogen-vacancy centers in diamond. *Phys. Rev. B* **81**, 035205 (2010).
184. Shields, B. J., Unterreithmeier, Q. P., De Leon, N. P., Park, H. & Lukin, M. D. Efficient readout of a single spin state in diamond via spin-to-charge conversion. *Phys. Rev. Lett.* **114**, 136402 (2015).
185. Jiang, L. et al. Repetitive readout of a single electronic spin via quantum logic with nuclear spin ancillae. *Science* **326**, 267–272 (2009).
186. Hopper, D., Shulevitz, H. & Bassett, L. Spin readout techniques of the nitrogen-vacancy center in diamond. *Micromachines* **9**, 437 (2018).
187. Siyushev, P. et al. Photoelectrical imaging and coherent spin-state readout of single nitrogen-vacancy centers in diamond. *Science* **363**, 728–731 (2019).
188. Niethammer, M. et al. Coherent electrical readout of defect spins in silicon carbide by photo-ionization at ambient conditions. *Nat. Commun.* **10**, 5569 (2019).
189. Acosta, V. M. et al. Dynamic stabilization of the optical resonances of single nitrogen-vacancy centers in diamond. *Phys. Rev. Lett.* **108**, 206401 (2012).
190. Anderson, C. P. et al. Electrical and optical control of single spins integrated in scalable semiconductor devices. *Science* **366**, 1225–1230 (2019).
191. Lee, D., Lee, K. W., Cady, J. V., Ovartchaiyapong, P. & Jayich, A. C. B. Topical review: spins and mechanics in diamond. *J. Opt.* **19**, 033001 (2017).
192. Macquarrie, E. R., Gosavi, T. A., Jungwirth, N. R., Bhave, S. A. & Fuchs, G. D. Mechanical spin control of nitrogen-vacancy centers in diamond. *Phys. Rev. Lett.* **111**, 227602 (2013).
193. Tchebotareva, A. et al. Entanglement between a diamond spin qubit and a photonic time-bin qubit at telecom wavelength. *Phys. Rev. Lett.* **123**, 063601 (2019).
194. Heremans, F. J., Yale, C. G. & Awschalom, D. D. Control of spin defects in wide-bandgap semiconductors for quantum technologies. *Proc. IEEE* **104**, 2009–2023 (2016).
195. Awschalom, D. D., Hanson, R., Wrachtrup, J. & Zhou, B. B. Quantum technologies with optically interfaced solid-state spins. *Nat. Photonics* **12**, 516–527 (2018).
196. Atatüre, M., Englund, D., Vamivakas, N., Lee, S.-Y. & Wrachtrup, J. Material platforms for spin-based photonic quantum technologies. *Nat. Rev. Mater.* **3**, 38–51 (2018).
197. Weber, J. R. et al. Quantum computing with defects. *Proc. Natl Acad. Sci. USA* **107**, 8513–8518 (2010).
198. Bassett, L. C., Alkauskas, A., Exarhos, A. L. & Fu, K.-M. C. Quantum defects by design. *Nanophotonics* **8**, 1867–1888 (2019).
199. Steinert, S. et al. High sensitivity magnetic imaging using an array of spins in diamond. *Rev. Sci. Instrum.* **81**, 043705 (2010).
200. Staudacher, T. et al. Nuclear magnetic resonance spectroscopy on a (5-nanometer) 3 sample volume. *Science* **339**, 561–563 (2013).
201. Kucsko, G. et al. Nanometre-scale thermometry in a living cell. *Nature* **500**, 54–58 (2013).
202. Chu, Y. et al. Coherent optical transitions in implanted nitrogen vacancy centers. *Nano Lett.* **14**, 1982–1986 (2014).
203. Maurer, P. C. et al. Room-temperature quantum bit memory exceeding one second. *Science* **336**, 1283–1286 (2012).
204. Evans, R. E., Sipahigil, A., Sukachev, D. D., Zibrov, A. S. & Lukin, M. D. Narrow-linewidth homogeneous optical emitters in diamond nanostructures via silicon ion implantation. *Phys. Rev. Appl.* **5**, 044010 (2016).
205. Rogers, L. J. et al. All-optical initialization, readout, and coherent preparation of single silicon-vacancy spins in diamond. *Phys. Rev. Lett.* **113**, 263602 (2014).
206. Nguyen, C. T. et al. Quantum network nodes based on diamond qubits with an efficient nanophotonic interface. *Phys. Rev. Lett.* **123**, 183602 (2019).
207. Nguyen, C. T. et al. An integrated nanophotonic quantum register based on silicon-vacancy spins in diamond. *Phys. Rev. B* **100**, 165428 (2019).
208. Sohn, Y.-I. et al. Controlling the coherence of a diamond spin qubit through its strain environment. *Nat. Commun.* **9**, 2012 (2018).
209. Iwasaki, T. et al. Tin-vacancy quantum emitters in diamond. *Phys. Rev. Lett.* **119**, 253601 (2017).
210. Trusheim, M. E. et al. Lead-related quantum emitters in diamond. *Phys. Rev. B* **99**, 075430 (2019).
211. Siyushev, P. et al. Optical and microwave control of germanium-vacancy center spins in diamond. *Phys. Rev. B* **96**, 081201 (2017).
212. Trusheim, M. E. et al. Transform-limited photons from a coherent tin-vacancy spin in diamond. *Phys. Rev. Lett.* **124**, 023602 (2020).
213. Rose, B. C. et al. Observation of an environmentally insensitive solid-state spin defect in diamond. *Science* **361**, 60–63 (2018).
214. Green, B. L. et al. Neutral silicon-vacancy center in diamond: spin polarization and lifetimes. *Phys. Rev. Lett.* **119**, 096402 (2017).
215. Rose, B. C. et al. Strongly anisotropic spin relaxation in the neutral silicon vacancy center in diamond. *Phys. Rev. B* **98**, 235140 (2018).
216. Li, Q., Davanço, M. & Srinivasan, K. Efficient and low-noise single-photon-level frequency conversion interfaces using silicon nanophotonics. *Nat. Photonics* **10**, 406–414 (2016).
217. Lukin, D. M. et al. 4H-silicon-carbide-on-insulator for integrated quantum and nonlinear photonics. *Nat. Photonics* **14**, 330–334 (2020).
218. Lohrmann, A., Johnson, B. C., McCallum, J. C. & Castelletto, S. A review on single photon sources in silicon carbide. *Rep. Prog. Phys.* **80**, 034502 (2017).
219. Son, N. T. et al. Developing silicon carbide for quantum spintronics. *Appl. Phys. Lett.* **116**, 190501 (2020).
220. Christle, D. J. et al. Isolated electron spins in silicon carbide with millisecond coherence times. *Nat. Mater.* **14**, 160–163 (2015).
221. Bourassa, A. Entanglement and control of single nuclear spins in isotopically engineered silicon carbide. *Nat. Mater.* **19**, 1319–1325 (2020).
222. Zargaleh, S. A. Evidence for near-infrared photoluminescence of nitrogen vacancy centers in 4H-SiC. *Phys. Rev. B* **94**, 060102 (2016).
223. Wolfowicz, G. et al. Vanadium spin qubits as telecom quantum emitters in silicon carbide. *Sci. Adv.* **6**, eaaz1192 (2020).
224. Crook, A. L. et al. Purcell enhancement of a single silicon carbide color center with coherent spin control. *Nano Lett.* **20**, 3427–3434 (2020).
225. Lukin, D. M. et al. Spectrally reconfigurable quantum emitters enabled by optimized fast modulation. *Npj Quantum Inf.* **6**, 80 (2020).
226. Thiel, C., Böttger, T. & Cone, R. Rare-earth-doped materials for applications in quantum information storage and signal processing. *J. Lumin.* **131**, 353–361 (2011).
227. Zhong, T. et al. Nanophotonic rare-earth quantum memory with optically controlled retrieval. *Science* **357**, 1392–1395 (2017).
228. Zhong, T. et al. Optically addressing single rare-earth ions in a nanophotonic cavity. *Phys. Rev. Lett.* **121**, 183603 (2018).
229. Kornher, T. et al. Sensing individual nuclear spins with a single rare-earth electron spin. *Phys. Rev. Lett.* **124**, 170402 (2020).
230. McAuslan, D. L., Bartholomew, J. G., Sellars, M. J. & Longdell, J. J. Reducing decoherence in optical and spin transitions in rare-earth-metal-ion-doped materials. *Phys. Rev. A* **85**, 032339 (2012).
231. Phenicie, C. M. et al. Narrow optical line widths in erbium implanted in TiO_2. *Nano Lett.* **19**, 8928–8933 (2019).
232. Kornher, T. et al. Production yield of rare-earth ions implanted into an optical crystal. *Appl. Phys. Lett.* **108**, 053108 (2016).
233. Ferrenti, A. M., de Leon, N. P., Thompson, J. D. & Cava, R. J. Identifying candidate hosts for quantum defects via data mining. *Npj Comput. Mater.* **6**, 126 (2020).
234. Andrich, P. et al. Microscale-resolution thermal mapping using a flexible platform of patterned quantum sensors. *Nano Lett.* **18**, 4684–4690 (2018).
235. Knowles, H. S., Kara, D. M. & Atatüre, M. Observing bulk diamond spin coherence in high-purity nanodiamonds. *Nat. Mater.* **13**, 21–25 (2014).
236. Boudou, J.-P. et al. High yield fabrication of fluorescent nanodiamonds. *Nanotechnology* **20**, 235602 (2009).
237. Andrich, P. et al. Engineered micro- and nanoscale diamonds as mobile probes for high-resolution sensing in fluid. *Nano Lett.* **14**, 4959–4964 (2014).
238. Beke, D. et al. Room-temperature defect qubits in ultrasmall nanocrystals. *J. Phys. Chem. Lett.* **11**, 1675–1681 (2020).
239. Trusheim, M. E. et al. Scalable fabrication of high purity diamond nanocrystals with long-spin-coherence nitrogen vacancy centers. *Nano Lett.* **14**, 32–36 (2014).
240. Ryan, R. G. et al. Impact of surface functionalization on the quantum coherence of nitrogen-vacancy centers in nanodiamonds. *ACS Appl. Mater. Interfaces* **10**, 13143–13149 (2018).
241. Tsukahara, R. et al. Removing non-size-dependent electron spin decoherence of nanodiamond quantum sensors by aerobic oxidation. *ACS Appl. Nano Mater.* **2**, 3701–3710 (2019).
242. Barry, J. F. et al. Sensitivity optimization for NV-diamond magnetometry. *Rev. Mod. Phys.* **92**, 015004 (2020).
243. Liu, Y.-X., Ajoy, A. & Cappellaro, P. Nanoscale vector dc magnetometry via ancilla-assisted frequency up-conversion. *Phys. Rev. Lett.* **122**, 100501 (2019).
244. Schloss, J. M., Barry, J. F., Turner, M. J. & Walsworth, R. L. Simultaneous broadband vector magnetometry using solid-state spins. *Phys. Rev. Appl.* **10**, 034044 (2018).

245. Balasubramanian, G. et al. Ultralong spin coherence time in isotopically engineered diamond. *Nat. Mater.* **8**, 383–387 (2009).
246. Laraoui, A. et al. Imaging thermal conductivity with nanoscale resolution using a scanning spin probe. *Nat. Commun.* **6**, 8954 (2015).
247. Pelliccione, M. et al. Scanned probe imaging of nanoscale magnetism at cryogenic temperatures with a single-spin quantum sensor. *Nat. Nanotechnol.* **11**, 700–705 (2016).
248. Zhou, T. X., Stöhr, R. J. & Yacoby, A. Scanning diamond NV center probes compatible with conventional AFM technology. *Appl. Phys. Lett.* **111**, 163106 (2017).
249. Fukami, M. et al. All-optical cryogenic thermometry based on nitrogen-vacancy centers in nanodiamonds. *Phys. Rev. Appl.* **12**, 014042 (2019).
250. Nguyen, C. T. et al. All-optical nanoscale thermometry with silicon-vacancy centers in diamond. *Appl. Phys. Lett.* **112**, 203102 (2018).
251. Anisimov, A. N. et al. Optical thermometry based on level anticrossing in silicon carbide. *Sci. Rep.* **6**, 33301 (2016).
252. Myers, B. A. et al. Probing surface noise with depth-calibrated spins in diamond. *Phys. Rev. Lett.* **113**, 027602 (2014).
253. Fávaro de Oliveira, F. et al. Tailoring spin defects in diamond by lattice charging. *Nat. Commun.* **8**, 15409 (2017).
254. Sangtawesin, S. et al. Origins of diamond surface noise probed by correlating single-spin measurements with surface spectroscopy. *Phys. Rev. X* **9**, 031052 (2019).
255. Yao, N. et al. Scalable architecture for a room temperature solid-state quantum information processor. *Nat. Commun.* **3**, 800 (2012).
256. Serbyn, M. et al. Interferometric probes of many-body localization. *Phys. Rev. Lett.* **113**, 147204 (2014).
257. Cai, J., Retzker, A., Jelezko, F. & Plenio, M. B. A large-scale quantum simulator on a diamond surface at room temperature. *Nat. Phys.* **9**, 168–173 (2013).
258. Abobeih, M. H. et al. Atomic-scale imaging of a 27-nuclear-spin cluster using a quantum sensor. *Nature* **576**, 411–415 (2019).
259. Choi, S. et al. Observation of discrete time-crystalline order in a disordered dipolar many-body system. *Nature* **543**, 221–225 (2017).
260. Zu, C. et al. Experimental realization of universal geometric quantum gates with solid-state spins. *Nature* **514**, 72–75 (2014).
261. Bernien, H. et al. Heralded entanglement between solid-state qubits separated by three metres. *Nature* **497**, 86–90 (2013).
262. Dréau, A., Tcheborateva, A., Mahdaoui, A. E., Bonato, C. & Hanson, R. Quantum frequency conversion of single photons from a nitrogen-vacancy center in diamond to telecommunication wavelengths. *Phys. Rev. Appl.* **9**, 064031 (2018).
263. Sipahigil, A. et al. Indistinguishable photons from separated silicon-vacancy centers in diamond. *Phys. Rev. Lett.* **113**, 113602 (2014).
264. Sipahigil, A. et al. An integrated diamond nanophotonics platform for quantum-optical networks. *Science* **354**, 847–850 (2016).
265. Evans, R. E. et al. Photon-mediated interactions between quantum emitters in a diamond nanocavity. *Science* **362**, 662–665 (2018).
266. Zhang, Z.-H. et al. Optically detected magnetic resonance in neutral silicon vacancy centers in diamond via bound exciton states. *Phys. Rev. Lett.* **125**, 237402 (2020).
267. Santori, C. et al. Nanophotonics for quantum optics using nitrogen-vacancy centers in diamond. *Nanotechnology* **21**, 274008 (2010).
268. Bhaskar, M. K. et al. Experimental demonstration of memory-enhanced quantum communication. *Nature* **580**, 60–64 (2020).
269. Degen, C. L., Reinhard, F. & Cappellaro, P. Quantum sensing. *Rev. Mod. Phys.* **89**, 035002 (2017).
270. Connors, E. J., Nelson, J., Qiao, H., Edge, L. F. & Nichol, J. M. Low-frequency charge noise in Si/SiGe quantum dots. *Phys. Rev. B* **100**, 165305 (2019).
271. Mi, X., Kohler, S. & Petta, J. R. Landau-Zener interferometry of valley-orbit states in Si/SiGe double quantum dots. *Phys. Rev. B* **98**, 161404 (2018).
272. Dial, O. et al. Charge noise spectroscopy using coherent exchange oscillations in a singlet-triplet qubit. *Phys. Rev. Lett.* **110**, 146804 (2013).
273. Kim, D. et al. Microwave-driven coherent operation of a semiconductor quantum dot charge qubit. *Nat. Nanotechnol.* **10**, 243–247 (2015).
274. Yang, C. et al. Silicon qubit fidelities approaching incoherent noise limits via pulse engineering. *Nat. Electron.* **2**, 151–158 (2019).
275. Rong, X. et al. Experimental fault-tolerant universal quantum gates with solid-state spins under ambient conditions. *Nat. Commun.* **6**, 8748 (2015).
276. Glenn, D. R. et al. High-resolution magnetic resonance spectroscopy using a solid-state spin sensor. *Nature* **555**, 351–354 (2018).
277. Simin, D. et al. Locking of electron spin coherence above 20 ms in natural silicon carbide. *Phys. Rev. B* **95**, 161201 (2017).
278. Michl, J. et al. Robust and accurate electric field sensing with solid state spin ensembles. *Nano Lett.* **19**, 4904–4910 (2019).
279. Volk, C., Chatterjee, A., Ansaloni, F., Marcus, C. M. & Kuemmeth, F. Fast charge sensing of Si/SiGe quantum dots via a high-frequency accumulation gate. *Nano Lett.* **19**, 5628–5633 (2019).

Acknowledgements

A.C and F.K. acknowledge support from the European Union's Horizon 2020 research and innovation programme under grant agreement nos. 688539 and 951852. A.C. acknowledges support from the EPSRC Doctoral Prize Fellowship. S.D.F. acknowledges support from the European Union, through the Horizon 2020 research and innovation programme (grant agreement no. 810504) and from the Agence Nationale de la Recherche, through the CMOSQSPIN project (ANR-17-CE24-0009). A.M. acknowledges funding from the Australian Research Council (projects CE170100012 and DP180100969), the U.S. Army Research Office (grant no. W911NF-17-1-0200) and the Australian Department of Industry, Innovation and Science (grant no. AUSMURI00002). F.K. acknowledges support from the Independent Research Fund Denmark. N.d.L. acknowledges support from the NSF under the EFRI ACQUIRE programme (grant 1640959) and the CAREER programme (grant no. DMR-1752047), the Air Force Office of Scientific Research (award numbers FA9550-17-0158 and FA9550-18-1-0334), the Eric and Wendy Schmidt Transformative Technology Fund and the Princeton Catalysis Initiative.

Author contributions

The authors contributed equally to all aspects of the article.

Competing interests

The authors declare no competing interests.

Peer review information

Nature Reviews Physics thanks the anonymous reviewers for their contribution to the peer review of this work.

Publisher's note